課程博士

学位授与年月　平成 29 年 03 月

関西大学審査学位論文

Studies on Physical and Chemical Property of ZnO Films and their Stability

（ZnO 薄膜の物理学的及び化学的特性とその安定性に関する研究）

理工学研究科　総合理工学専攻

機能性材料・デバイス

14D6001・　張捷生

博士論文要旨

理工研究科　総合理工学専攻
機能性材料・デバイス
14D6001
張捷生

論題：”Studies on Physical and Chemical Property of ZnO Films and their Stability”
（ZnO 薄膜の物理学的及び化学的特性とその安定性に関する研究）

論文概要

２０世紀後半のエネルギー消費を支えた化石燃料の消耗が危惧されて以来、安定な代替えエネルギー源として原子力発電がクリーン・エネルギーとして有望視され、世界中で原子炉の建設が進んだ。他方で、再生可能エネルギー源として太陽電池の研究も着実に進められてきた。

日本においても、同様の潮流が続き、国内に数十基の原子炉を抱えている。しかしながら２０１１年３月の東日本大震災で被災した東京電力福島第一原発のメルトダウン事故を契機に、原子力発電の安全性に対する危惧と総コストに対する考え方の見直し議論を経て、国内では原子力エネルギーへの依存度を削減する方向で施策が変更されようとしている。

日本では、再生エネルギー技術の一つとして風力発電所の建設も進んでいるが、歴史的背景を踏まえた技術成熟度からみてソーラーパワーの活用が現実的であるとみられている。今世紀に入ってから家庭用の発電システムの低価格化が進み、政府の電力買い上げ政策も進められてきた。それゆえ、時間はかかるものの、着実に普及が進むと予測される。

このような背景にあって、ソーラーパネルのエネルギー収率を高めるために透明電極が当たり前のように適用されてきたが、従来の主たる素材である ITO の毒性が指摘されてから代替え電極材料の研究が加速されてきた。典型的な材料として亜鉛酸化物（ZnO）が取り上げられ、膜の低抵抗化の検討が広く行われてきた。元々ZnO は古くから知られているセラミック半導体であり、その物理学的、化学的性質などはよく理解されていると考えられていた。従って低抵抗化のためのドーピング手法も早期に解決し、技術的課題は少ないと考えられてきた。しかしながら、ZnO 膜の伝導を担う電子の発生機構について解釈が不明瞭であり、酸素空孔との関係が第一原理計算によっても明らかにはされていない。

それゆえ、今後の透明電極材料としての技術的発展を確かなものにするためには、基本的な伝導機構の解明が不可欠であり、この点の解明は十分に価値のある研究課題であるといえる。

上記のような学術的背景に基づき、本学位論文では、いくつかの手法によってノンドープ ZnO 膜（以下単に ZnO 膜と呼ぶ）と Al ドープ ZnO 膜（以下 AZO 膜と呼ぶ）を形成して膜の物理的及び化学的性質を評価しながら、伝導機構を支配している本質に迫る。

第一章では、本学位論文の位置づけとして研究の背景が述べられている。

第二章では、ZnO 膜および AZO 膜形成技術としてスピンコート法とスパッタ法の基本的な考え方を説明すると共に、本論文で採用した具体的な成膜条件などについても、その特徴を説明している。

第三章では、最初に検討したスピンコート法によって形成した ZnO 膜と AZO 膜の電気的、光学的な

特性が成膜条件によってどのように変化し、好ましい特性を得るにはどのような成膜条件が不可欠であるかを議論している。熱処理雰囲気と熱処理温度条件の選択が共に重要な意味を持つことが明らかにされるが、十分な光学的透過特性が得にくいことも示されている。

第四章では、スパッタ法によって形成した ZnO 膜の電気的特性が決まる機構を詳細に調べている。ドーピングによる電気的特性の制御以前に、そもそもノンドープ ZnO 膜の電気伝導特性がどのように決まるかが必ずしも明確にされていないことから、伝導性の制御にはこの点を明らかにする努力が不可欠であると考え、物理学的、或いは化学的な分析によって薄膜の伝導機構を調べている。

伝導機構を支える主要パラメータの一つとして膜中の電子濃度に注目し、酸素空孔の発生が電子生成をもたらすとされる従来からの考え方がどの程度適切かを酸素の化学的結合状態の分析を通じて考察している。ZnO 膜の堆積条件とその後の熱処理によって膜中の酸素量に大きな変化がないにもかかわらず、膜中の電子濃度が製造条件に依存して著しく変化することが明らかとなった。この事実は、膜中酸素空孔量と膜中酸素濃度が直接関係するであろうとする従来の考え方に疑問を抱かせる。この点を XPS 法により O1s スペクトルの解析から明らかにしようとしたが、従来の二成分分解法では、O1s のサブスペクトル強度と電子濃度に全く対応関係が存在しないことが明確になり、最近注目されている三成分分解法挑戦している。O1s スペクトル成分強度と電子濃度は逆の関係にあり、当初この成分が酸素空孔量に関係するとされたすでに公表された解釈は矛盾することを明らかにしている。むしろ、ZnO 膜のマトリクス構造中の酸素イオン（O^{2-}）に関係づけられるとする考え方のほうが適切であることが想定された。根拠は、ZnO 膜堆積時に雰囲気として安定酸素同位体(O^{18})を使った実験により与えられた。即ち、当初 ZnO を構成していた O^{18} は、堆積後に N_2 雰囲気の熱処理を行っても O_2 雰囲気の熱処理を行っても減少する。他方で同時に存在する O^{16} はいずれの場合も減少しない。N_2 雰囲気熱処理を行った ZnO 膜は電子濃度が最も高く、O_2 雰囲気熱処理を行った ZnO 膜は電子濃度が最も低い。したがって、ZnO 膜中の O^{18} の減少は酸素空孔の発生増加だけを意味するわけではなく、ZnO から酸素原子が構造的にイオン化離脱していることを強く示唆している。これは、同位体酸素を使った今回の実験で初めて明らかにした。

第五章では、スパッタ法により堆積した ZnO 膜の長時間大気暴露による電気的特性の安定性を評価している。約 1 か月の暴露によって製造条件の異なる ZnO 膜の電気的特性を詳細に調べた結果、膜内部の化学的結合状態、膜の組成を含めて大きな変化が現れず、安定な特性を保持できることが明らかとなり、スパッタ法による ZnO 膜の良好な特性を確認している。

第六章では、前章までに述べてきた事柄を全体として整理している。

以上

Studies on Physical and Chemical Property of ZnO Films and their Stability

Jiesheng Zhang

March, 2017

INDEX

Chapter 1. BACKGROUND OF THE STUDY

1.1 Current Status of Electrical Energy

Electric energy is always produced through some form of energy conversion; energy is converted from one form such as potential energy, kinetic energy, or chemical energy into electricity [1].

1.1.1 Sources of energy

Electricity is produced by converting energy from one form into electricity. This conversion may involve mass-less conversion, where the energy source is converted directly into electricity. For example, solar photovoltaic cells convert the energy present in solar radiation, directly into electricity [2]. On the other hand, the mass conversion process utilizes the energy present in one form, via an intermediate form, into electricity. Coal-plants are well-known example of the mass process, where the coal is burnt to access its chemical energy which used to raise the kinetic energy of rotating steam turbines which tapped to generate electricity electro-magnetically [3]. The majority of electricity today is produced by some form of mass energy conversion process [4]. Mass-less and mass-based systems use the following major sources of energy for the production of electricity: fossil fuels, uranium fuel, solar radiation, and hydroenergy [5].

Fossil fuels include coal, petroleum, and natural gas, all of which are basically finite, non-renewable resources. They are modern primary sources for the production of electricity. The combustion of these fuels releases their chemical energy, which produces heat to drive steam turbines and their attached electric generators, resulting in the conversion of kinetic energy into electricity [6]. No energy conversion process is available that converts all the energy present in one form completely into the desired form of electricity. Since the production of electricity from fossil fuels involves several physical and energy conversion steps, fossil fuel power plants are inefficient at producing power (at most around 40%). Table 1.1 summarizes the energy content of fossil fuels and an estimation of current fossil fuel reserves in the world [7].

Table 1.1 Estimate of Fossil-Fuel Energy Content and World Fossil Fuel Reserve [7]

Fuel	Approx. Energy Content (Watts/yrs)	Estimated Reserves
Coal	937/ton	7.6 trillion metric tons
Petroleum	168/barrel	2 trillion barrels
Natural Gas	$0.036/ft^3$	$10^{16} ft^3$

We must also consider the environmental effects of generating electricity from fossil fuels. For example, flyash, which is the physical matter left after coal combustion, is dangerous to not only our health, but also to many animals and the environment [8]. Disposing of flyash in an environmentally friendly manner is extremely difficult. Combusting fossil fuels also produces carbon monoxide, carbon dioxide, sulfur dioxide, and other harmful gases [9]. It is anticipated that these "greenhouse gases" contribute to generation of acid rain and global warming [10].

Nuclear energy, like fossil fuels, is a finite, non-renewable energy source that applies a mass conversion process to produce electricity [11]. There are two basic forms of nuclear energy, fission and fusion [12]. Since the fusion technique is not yet viable for producing electricity, only fission is used to produce electricity. The fission reaction involves splitting the nuclei of heavy elements. The thermal energy release by these nuclear reactions powers steam turbines with attendant electric generators, just as in a fossil fuel power plant. Nuclear fission has greater energy density than fossil fuels. Uranium effectively contains energy of approximately 10^{10} Btu/kg, which is about one million times higher than the chemical energy of fossil fuels [13]. There is an estimated reserve of approximately 426 million kg of uranium in the United States. Nuclear fission also comes with heavy environmental costs and risks. The fission process leaves toxic blend of nuclear fuel, the reactor vessel containing the fission process and the steam pipes become highly radioactive. In addition, plant failures can lead to the release of radioactive steam and particulates into the atmosphere or worse.

Many energy sources are used to produce our current diverse range of electrical sources. Non-renewable energy source includes nuclear and fossil fuels. Renewable energy sources range from direct solar (photovoltaic cells) to more indirect solar (steam production by solar heating) and geothermal energy. Most renewable sources are site specific, such as hydroelectricity, wind power, and tidal power [14]. All renewable energy sources have some of handicap or another, and the social good comes with costs to the environment and the future.

1.1.2 Environmental impact of electricity generation

All methods used to produce electricity today have one or more environmental impacts [15]. The impact may be active like the emission of airborne pollutants, or may be passive like aesthetics or habitat modification. Electricity generation must be reconsidered in light of the environmental impact possible. This includes the production and transportation of fuel used in the conversion process [16]. This thesis focuses on the environmental impact of electricity production. Such impacts are most obvious with fossil fuel and nuclear power plants, which extract large quantities of fuel from the earth. Power plant emissions of typical methods, which are discussed below, are summarized in Figure 1.1 [17].

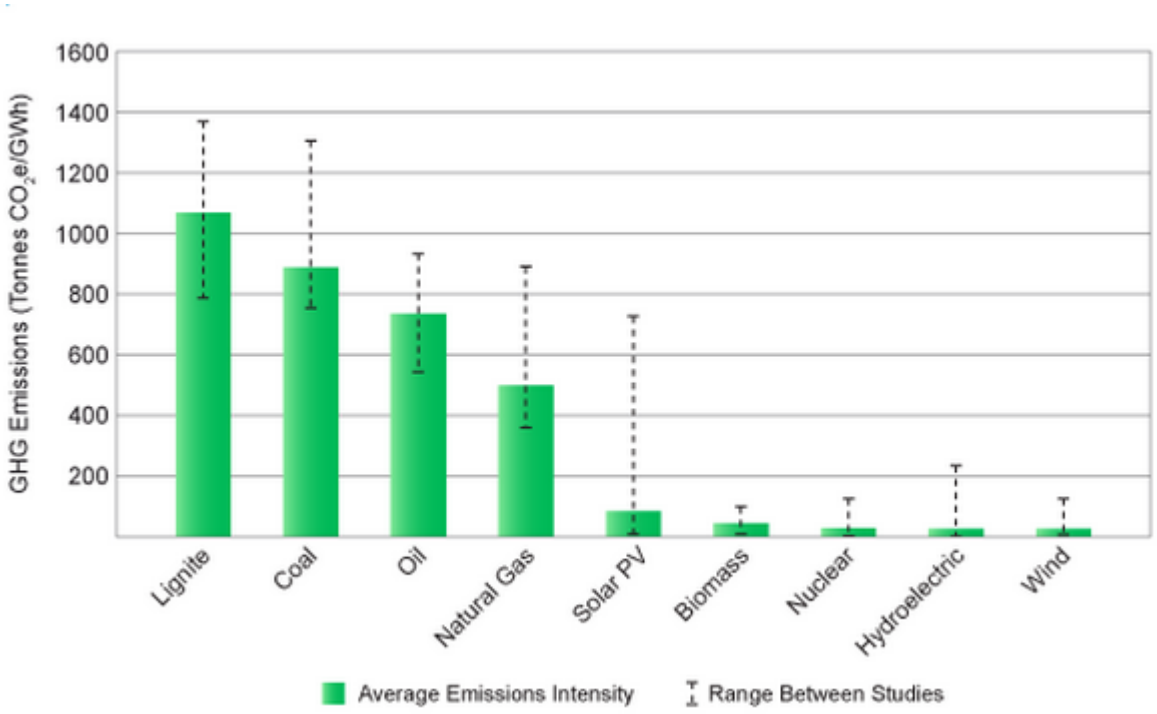

Figure 1.1. Power Plant Emissions (Tones CO_2/GWh) [17]

Coal Production

Coal is almost exclusively mined for generating electricity. Coal production is often viewed as just a local environmental problem. Coal mining, particularly surface mining, has both long-term and short-term effects on the land, including dust, noise, and water drainage/runoff. The preparation of coal produces huge quantities of solid and liquid wastes, which must be chemically treated and disposed of safely.

Oil Production

The fuel oil burned in power plants is a byproduct of the petroleum industry, so electricity production is partially responsible for the environmental issues associated with the consumption of oil and hydrocarbon. Burning fuel oil produces many "greenhouse" gases. Other environmental impacts associated with oil production include blowouts, spills, brine disposal, ground instability, and the production of hydrogen sulfide.

Natural Gas Production

During natural gas production, possible damages to the environment include blowouts, leaks, hydrocarbon emissions, and trace metal emissions. The treatment of natural gas yields air emissions and the disposal of liquid residuals, while transportation and storage effects include spills and explosions.

1.1.3 Green Energy Source - Solar Cell

Solar radiation is a renewable energy source. The average incident power at the earth's surface is 182 W/m^2, which corresponds to a daily average energy supply of 4.4 kWh/m^2 [18]. Direct use of solar power includes active systems involving photovoltaic cells, and passive systems that use solar collectors to gather radiation and raise steam. Photovoltaic cells directly convert sunlight into electricity. The best photovoltaic cells to date have efficiencies in the 14% to 17% range [19]. Environmentally attractive, they have no emissions, minimal wasteful by-products, and minimal mass utilization. However, the most efficient solar cells use gallium arsenide, a toxic material [20]. It seems that solar cells are too new for a proper understanding of the disposal requirements and costs posed by worn out cells. In addition, photovoltaic solar cells generate direct current,

and hence require invertors to obtain the alternating current desired for most large-scale consumers [21]. Solar collectors are normally incorporated into a solar thermal system, converting sunlight into heat for various forms of use, including space heating, water heating, industrial process steam generation, and electricity production [22]. At present, several factors limit the large-scale utilization of solar energy, including the cost of solar cells and solar collector-heat exchanger systems, maintenance costs, and the need for adequate energy storage systems that can smooth out the daily variation. Yet, sunlight is found everywhere, making the use of solar radiation for energy production non-site specific.

The production of electricity from solar energy sources generally has only a small effect on the environment [23]. The energy conversion process has no by-products. Solar thermal systems are the sole exception as they have an operating fluid that must occasionally be replaced and the spent fluid discharged. There are some environmental concerns, however. Bulk solar plants generally require a large land area, and they tend to create heat islands. An unknown factor in solar energy is the disposal of photovoltaic cells. While the positives of photovoltaic cells far outweigh their negatives, continuous effort is needed to keep enhancing their efficiency and performance. Transparent conducting oxides (TCO), which are utilized as transparent electrodes in many types of thin film solar cells, are key determiners of both efficiency and performance.

TCO systems are found in Si thin film solar cells, such as CdTe thin film solar cells, and CIGS thin film solar cells [24]. For example, in Si thin film solar cells [25], as illustrated in Fig.1.2, the light trapping allows the thickness of the Si absorber layer to be reduced which paves the way for increased device stability. Therefore, using TCO layers as transparent electrodes in Si solar cells is a key step in raising device performance. Details of TCO characteristics are given below.

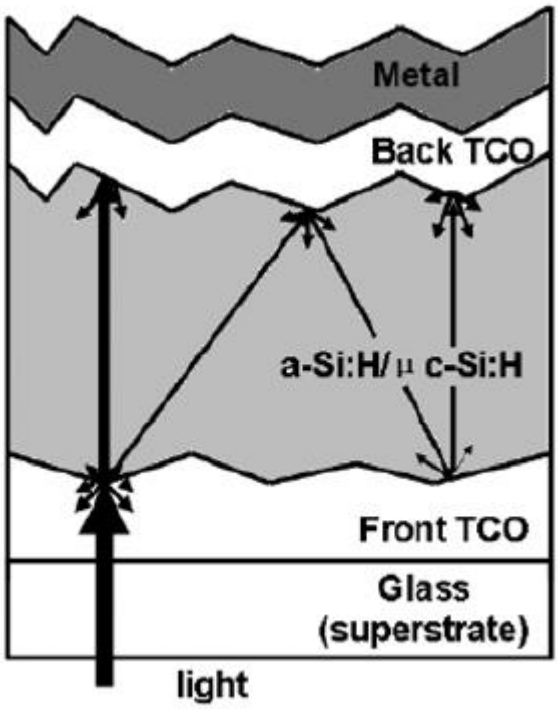

Figure 1.2. A schematic sketch of a Si solar cell with front and back TCO contact layers [25].

1.2 Properties of Transparent Conductive Oxides (TCO)

Transparent conductive oxides (TCO), most often doped metal oxides, are used in optoelectronic devices such as flat panel displays and photovoltaic devices (including inorganic devices, organic devices, and dye-sensitized solar cells) because of they are transparent at visible wavelengths and have high electrical conductivity [26]. Most fabricated films have polycrystalline or amorphous microstructures. Typically used as electrode materials, they offer over 80% transmittance of incident light as well as electrical conductivity values higher than 10^3 S/cm and so permit efficient carrier transport [27]. In general, TCOs for thin-film electrodes in solar cells should have minimum carrier concentrations of the order of 10^{20} cm^{-3} for low resistivity with bandgaps greater than 3.2 eV to avoid the absorption of light over most of the solar spectrum [28]. Carrier mobility in these films is usually limited by ionized impurity scattering due to the large numbers of ionized donors in the film and is at most 40 $cm^2/V/s$ for the best TCOs. Current transparent conductive oxides used in industry are primarily n-type conductors, meaning that the primary carriers are electrons. This is because electron mobility is usually higher than hole mobility, and the difficulty of finding shallow acceptors in wide band gap oxides that can permit high hole concentrations. Suitable p-type transparent conductive oxides are still being researched, but the best of them still lies orders of magnitude behind n-type TCOs [29].

Today, the most important TCO material for electrode applications is In_2O_3, and the typical dopant is tin (In_2O_3:Sn = ITO). Tin-doped In_2O_3-based TCOs are been found to possess very good electrical and optical properties [30]. The smallest resistivity of Sn-doped In_2O_3 (ITO) is just below 10^{-4} Ωcm in the laboratory, with typical resistivity being about $1x10^{-4}$ Ωcm. The transparency is primarily ruled by the optical band gap, which is ≥3.3 eV, leading to transparency for wavelengths >360 nm. However, since In is a toxic material and very expensive (it is a rare metal), a search for alternative TCO films comparable to or better than ITO continues unabated [31].

Turning our attention to up and coming alternatives to ITO, we find ZnO (zinc oxide). It has an electron affinity of 4.35 eV and a direct band gap energy of 3.28 eV and is an n-type semiconductor material with the residual electron concentration of ~10^{17} cm^{-3} [32]. As doped ZnO films have been assumed to have very attractive electrical and optical properties for electrode applications, many dopants have been studied for ZnO-

based binary TCOs; *i.e.*, Ga, Al, B, In, Y, Sc, V, Si, Ge, Ti, Zr, Hf, and F have been examined [33]. Advantages of ZnO-based TCOs are low cost, abundant material resources, and non-toxicity. At present, ZnO films heavily doped with Ga and Al (dubbed GZO and AZO) have been demonstrated to have low resistivity and high transparency in the visible spectral range and, in some cases, even outperform ITO and FTO [34]. The dopant concentration in GZO or AZO usually lies in the range of 10^{20} to 10^{21} cm^{-3}. Although we have obtained GZO films with mobility of ~95 $cm^2/V/s$ in our laboratory, the typical mobility of GZO films reported is near or slightly below 50 $cm^2/V/s$. Ionization energies of Al and Ga donors (in the dilute limit which decreases with increased doping) are 53 and 55 meV, respectively, which are slightly lower than that of In (63 meV). Agura *et al*. reported a very low resistivity of ~8.5×10^{-5} Ωcm for AZO, and Park *et al*. reported a resistivity of ~8.1×10^{-5} Ωcm for GZO, both of which are similar to the lowest reported resistivity of ~7.7×10^{-5} Ωcm for ITO. AZO and GZO films can easily achieve transmittance values of 90% or more, which is comparable to the best value reported for ITO optimized for transparency alone, and far exceeds that of the traditional semitransparent thin Ni/Au metal electrodes (transmittance is below 70% in visible wavelengths) [35]. The high transparency of AZO and GZO originates from the wide band gap of ZnO. Low growth temperature of AZO or GZO has also intrigued researchers with respect to transparent electrode applications in solar cells. Compared to ITO, ZnO-based TCOs show better thermal stability of resistivity and better chemical stability at high temperatures, both of which bode well for the optoelectronic devices in which this material would be used [36]. In short, AZO and GZO are TCOs attracting more attention, if not the most, as ITO replacements. From the viewpoints of cost, availability, and environmental impact, AZO appears to be the best candidate. This conclusion is also bolstered by the availability of batch production of AZO films allowing large-area and large-scale production.

1.3 The Purpose of this Dissertation

Starting with an eye on production economies, I attempted to spin-coat ZnO and Al doped ZnO (AZO) thin films and tried to optimize the deposition and annealing conditions to achieve films with the best physical properties for TCO applications. Interestingly, I found that the films deposited by spin-coating had very higher

resistivity values making them unsuitable for TCO use. Since the reason for the high resistivity was not clear, I shifted the research target to the fundamental mechanism of carrier generation in ZnO films. I chose the RF sputtering method to get uniform and low resistivity films.

As the primary aim of the experiments was to elucidate the dominant mechanism controlling the electrical property of undoped ZnO films and impurity-doped ZnO films, it was necessary to clearly identify the structural aspects of undoped ZnO films. In some cases, I regarded the measured chemical and physical properties of ZnO as only rough estimates, rather than highly reliable values. Since the characteristics of ZnO films are expected to depend on fabrication conditions, I carefully investigated the various factors that might modify the structure and property of the films.

For this I characterized the oxygen-bonding state by X-ray photoelectron spectroscopy (XPS). In this dissertation, I propose an advanced method to characterize the relation between the oxygen-related spectrum component and the electron concentration. The relation between oxygen-bonding states and oxygen vacancy generation is discussed from various viewpoints of the films' electrical property. In addition, I trace the evolution of the in-depth concentration profile of oxygen isotope atoms captured by the ZnO films during deposition in order to elucidate how oxygen atoms and oxygen vacancies behave and contribute to electron generation. I reveal how the annealing condition after deposition changes the in-depth profile of oxygen atoms.

Chapter 2. THE DEPOSITION METHOD OF ZnO FILMS

ZnO films can be prepared by different techniques such as spray pyrolysis [37], pulse laser deposition [38], chemical vapor deposition [39], sol-gel [40] and magnetron sputtering methods [41]. In this Chapter, I will introduce the spin-coating method and the sputtering method both which were used in my research.

2.1 Spin-coating Method

The spin coating method is one of the most well-known techniques for applying thin films to substrates and is used in a wide variety of industries and technology sectors. The use of spin coating in organic electronics and nanotechnology is widespread and has built upon many of the techniques used in other semiconductor industries but also has some differences due to the relatively thin films. They include the high uniformity needed for effective device preparation, as well as the need for self-assembly and organization to occur during the casting process [42].

Spin coating generally involves the application of a thin film (a few nm to a few μm) evenly across the surface of the substrate by coating (casting) a solution of the desired material in a solvent while the substrate is rotated. The standard process is shown in Figure 2.1 [43]. First the substrate is coated in an ink containing the desired molecules dissolved in a solvent (1). The substrate is then rotated at high speed and most of the ink is flung off the sides (2). Airflow then removes most of the solvent leaving a plasticized film (3) before the film fully dries leaving the molecules on the surface (4).

The advantages of spin coating are its simplicity and relative ease with which a process can be set up coupled with the thin and uniform coatings that can be achieved. High spin speeds enhance the airflow yielding drying times which in turn results in high consistency at both macroscopic and nanometer scales. The disadvantage of spin coating is that it is an inherently batch (single substrate) process and thus relatively low throughput compared to roll-to-roll processes. The fast drying times can also lead to lower performance for some particular nano-technologies (small molecule OFETs for example) which require time to self-assemble and/or crystallize.

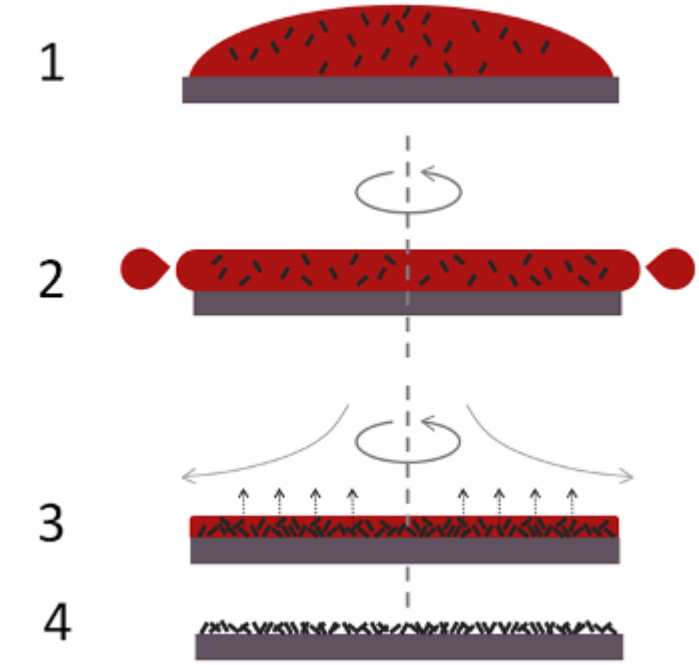

Figure 2.1. Example of spin coating a small molecule in solution using a static dispense [43].

Finally, material usage efficiency is typically very low at around 10% or less with most material being flung off the sides and wasted [44]. Whilst this is not usually an issue in research, it is clearly wasteful for manufacturing.

In general, the thickness of a spin coated film is proportional to the inverse of the spin speed squared as in the following equation, where *t* is the thickness and ω is the angular velocity [45]:

$$t \propto \frac{1}{\sqrt{\omega}} \qquad (2.1)$$

This means that film thickness will be halved if the rotation speed is quadrupled. A spin curve can also be calculated from this equation as follows. The exact thickness of a film will depend upon the material concentration and solvent evaporation rate (which in turn depends upon the solvent viscosity, vapor pressure, temperature and local humidity) and so for this reason, spin vs. thickness curves for new inks are most commonly determined empirically. Typically a test film is spin coated and the thickness is measured either by ellipsometry or surface profilometry. From this one or more data points, the spin vs. thickness curve can be calculated - usually with a good degree of accuracy. The spin speed can then be adjusted to give the desired film thickness.

In this experiment, I used the spin-coating method to obtain ZnO and AZO films. The Al/Zn atomic ratio of the AZO film in this solution was 1/50. The process of deposition is drawn in Figure 2.2. At first, the substrates were cleaned using the sequence of deionized water, methanol, acetone and deionized water by ultrasonic cleaning machine. Spin-coating was performed at room temperature, with a rate of 500 rpm for 5 sec and 2000 rpm for 20 sec. The deposited films were preheated at 120°C for 2 min and then were annealed at 500, 600, 700, or 800°C using an electric furnace for 60 min under an atmosphere of air and oxygen gas. The same coating process was repeated 9 times to obtain relatively uniform thick films [46].

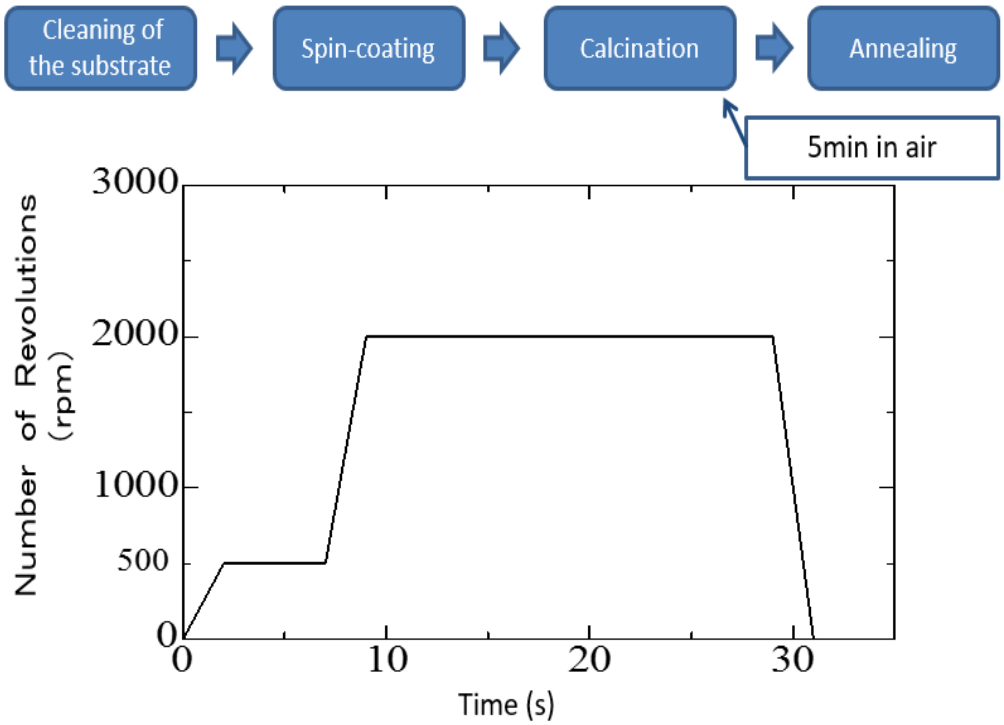

Figure 2.2. The process of spin-coating method [46]

2.2 Sputtering Method

Sputter deposition creates thin films by physical vapor deposition (PVD) [47]. This involves ejecting material from a "target", the source, onto a "substrate" such as a silicon wafer. Resputtering is re-emission of the deposited material during the deposition process by ion or atom bombardment. Sputtered atoms ejected from the target have a wide energy distribution, typically up to tens of eV (100,000 K). The sputtered ions (typically only a small fraction of the ejected particles are ionized — on the order of 1%) can ballistically fly from the target in straight lines and energetically impact the substrates or vacuum chamber walls (causing resputtering). Alternatively, at higher gas pressures, the ions collide with the gas atoms that act as a moderator and move diffusively, reaching the substrates or vacuum chamber wall and condensing after undergoing a random walk. The entire range of physical effects from high-energy ballistic impact to low-energy thermalized motion is accessible by changing the background gas pressure. The sputtering gas is often an inert gas such as argon. For efficient momentum transfer, the atomic weight of the sputtering gas should be close to the atomic weight of the target, so for sputtering light elements neon (Ne) is preferable, while for heavy elements krypton or xenon are used. Reactive gases can also be used to sputter compounds. The compound can be formed on the target surface, in-flight or on the substrate depending on the process parameters. The many parameters that control sputter deposition make it a complex process, but also allow experts a large degree of control over the growth and microstructure of the film [48].

Compared with other deposition methods, an important advantage of sputter deposition is that even materials with very high melting points can be easily formed as films whereas the evaporation of these materials in a resistance evaporator or Knudsen cell is problematic or impossible. Sputter deposited films have a composition close to that of the source material. The difference is due to different elements spreading differently because of their different mass (light elements are deflected more easily by the gas) but this difference is constant. Sputtered films typically have better adhesion to the substrate than evaporated films. The target contains a large amount of material and is maintenance free making the technique suited for ultrahigh vacuum applications. Sputtering sources contain no hot parts (to avoid heating they are typically water cooled) and are

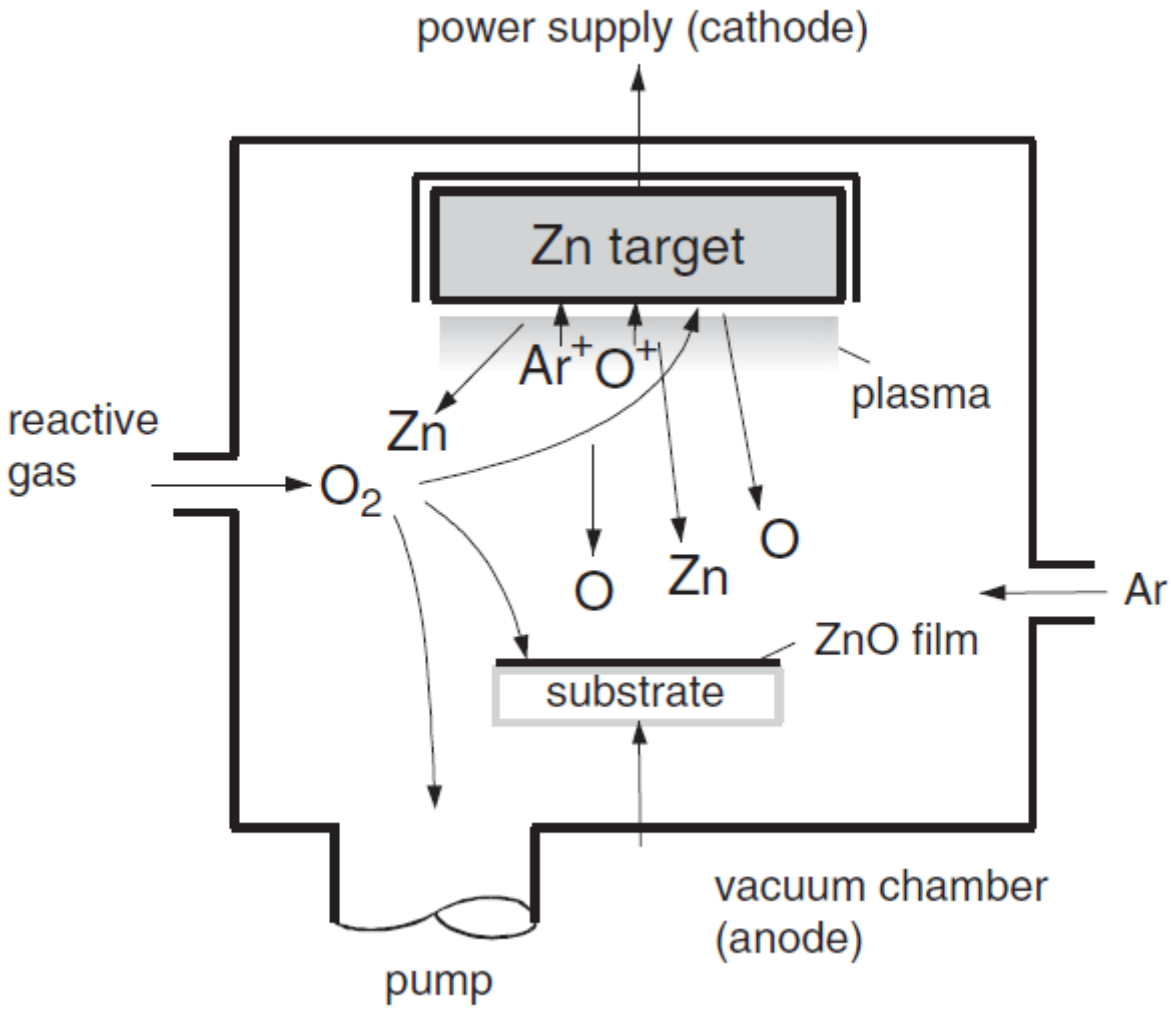

Figure 2.3. An example of sputtering deposition of ZnO by DC sputtering of a metallic Zn target in an Ar/O2 atmosphere [48].

compatible with reactive gases such as oxygen. Sputtering can be performed top-down while evaporation must be performed bottom-up. Advanced processes such as epitaxial growth are possible.

Some disadvantages of the sputtering process are that the process is more difficult to combine with a lift-off for structuring the film [49]. This is because the diffuse transport, characteristic of sputtering, makes a full shadow impossible. Thus, one cannot fully restrict where the atoms go, which can lead to contamination problems. In addition, an active control for layer-by-layer growth is difficult to implement compared to pulsed laser deposition and inert sputtering gases enter the film as it is deposited as impurities. Pulsed laser deposition is a variant of the sputtering deposition technique in which a laser beam is used for sputtering. The role of the sputtered and resputtered ions and the background gas has been fully investigated for the pulsed laser deposition process.

The simplest approach for the deposition of ZnO films by sputtering is sketched in Figure 2.3 [48]: A DC glow discharge is formed between a cathode, which is a planar Zn target, and the anode, which is the camber of the vacuum system. The system is pumped to a pressure of ~10 Pa and Ar and O_2 gasses are introduced into the vacuum chamber.

In this experiment, the substrate has a 100-nm-thick top SiO_2 film on a (001) p-type Si wafer. Before depositing the ZnO films, the substrates were chemically cleaned with sulfuric acid and hydrogen peroxide liquid for 3 min, followed by a rinse with de-ionized water. ZnO films were deposited on the top 100-nm-thick SiO_2 film by the RF sputtering technique. The RF power density was 1.99 W/cm^2. The distance between the substrate and the ZnO target was 50 mm. The base pressure was below $4x10^{-3}$ Pa. The ambient gas was composed of pure Ar or a mixture of Ar and O_2 gases (Ar: O_2 = 1:1). The gas pressure during the deposition was 0.66 Pa. The resulting ZnO films were about 75 nm thick. The samples were annealed at 700 C for 10, 30, or 60 min under an ambient gas of nitrogen or oxygen. Finally, circular Pt electrodes with area of 0.064 cm^2 were deposited, using shadow mask, by the electron beam evaporation technique to allow the evaluation of electrical characteristics. The distance between two Pt electrodes is 0.5 mm. The structure of samples used to characterize the electrical properties is overviewed in Fig. 2.4 [50].

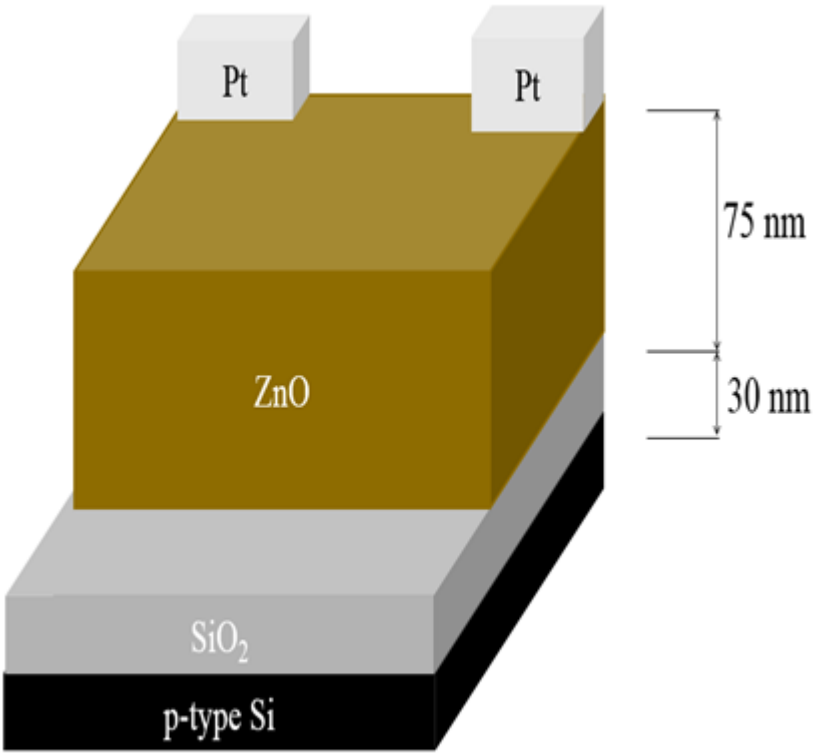

Figure 2.4. Bird's eye views of samples with top Pt electrodes [50].

Chapter 3. PROPERTIES OF ZnO THIN FILMS BY SPIN-COATING METHOD

In this Chapter, I will discuss the effect of annealing temperature on ZnO and Al-doped ZnO (AZO) thin films and also I try to find the deposition conditions that yield films with the best properties for TCOs. The crystal structure of the ZnO and AZO films were characterized by an X-ray diffractometer using CuK_{α} radiation (λ=0.15406nm) at an excitation voltage of 40kV and a current of 30mA. The thickness of the deposited films was measured by a film thickness monitor. The electrical resistivity, ρ, was measured at room temperature by the four-point probe method. The optical transmittance was recorded by a spectrophotometer in the visible range (400~700nm).

3.1 Effect on ZnO films

Figure 3.1(a) and 3.1(b) shows the XRD spectra of the ZnO films deposited on quartz substrates and annealed under oxygen and air, respectively. From Figure 3.1, it is found that the original ZnO films (no annealing), have no peak in any position, which means that the original ZnO thin films have an amorphous structure. At the other hand, the annealed ZnO films show strong peaks 2θ=31.72, 34.45 and 36.21˚ positions regardless of the atmosphere. These peaks correspond to ZnO planes of (100), (002) and (101) [51]. It is also found that all annealed ZnO films exhibited the strongest peak from their (002) preferred orientation. Since ZnO has the wurtzite structure, which is depicted in Figure 3.2 [52], these results confirm that with annealing, the spin-coating method can create ZnO films with Z-axis orientation. However, the peak variation of the (002) plane exhibited some dependency on annealing temperature. When the annealing temperature was increased from 400 ℃ to 600 ℃, the peak intensity of the (002) plane increased, but when the annealing temperature was increased from 600 ℃ to 700 ℃, the peak intensity of the (002) plane fell, which suggest that ZnO film crystallization peaked at around 600℃.

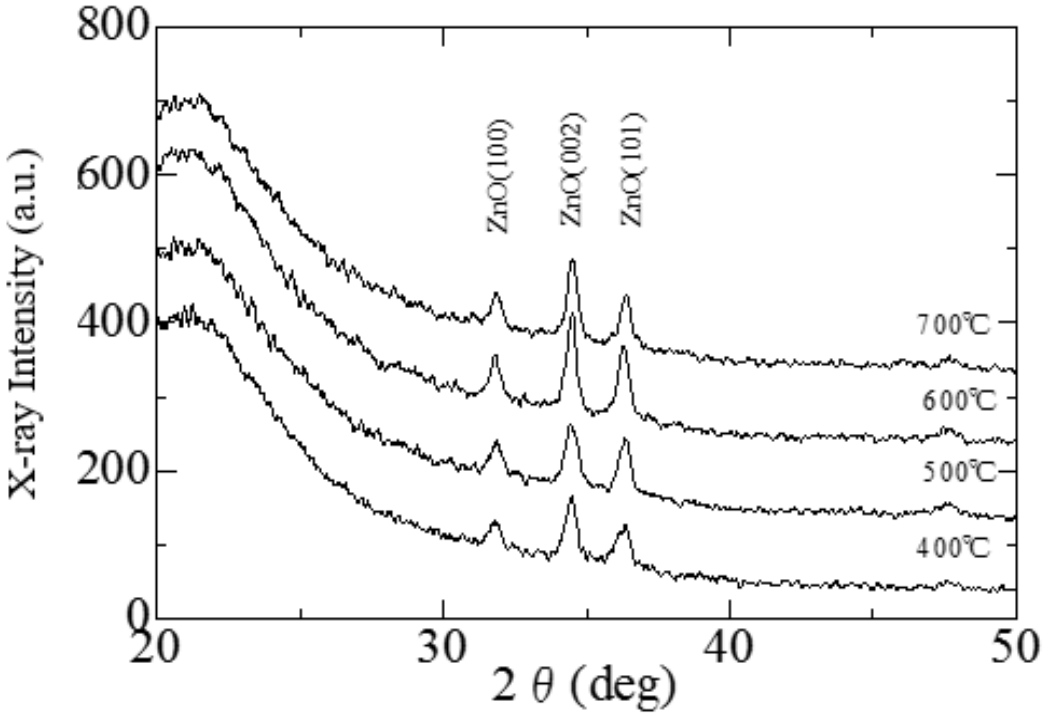

(a) Oxygen

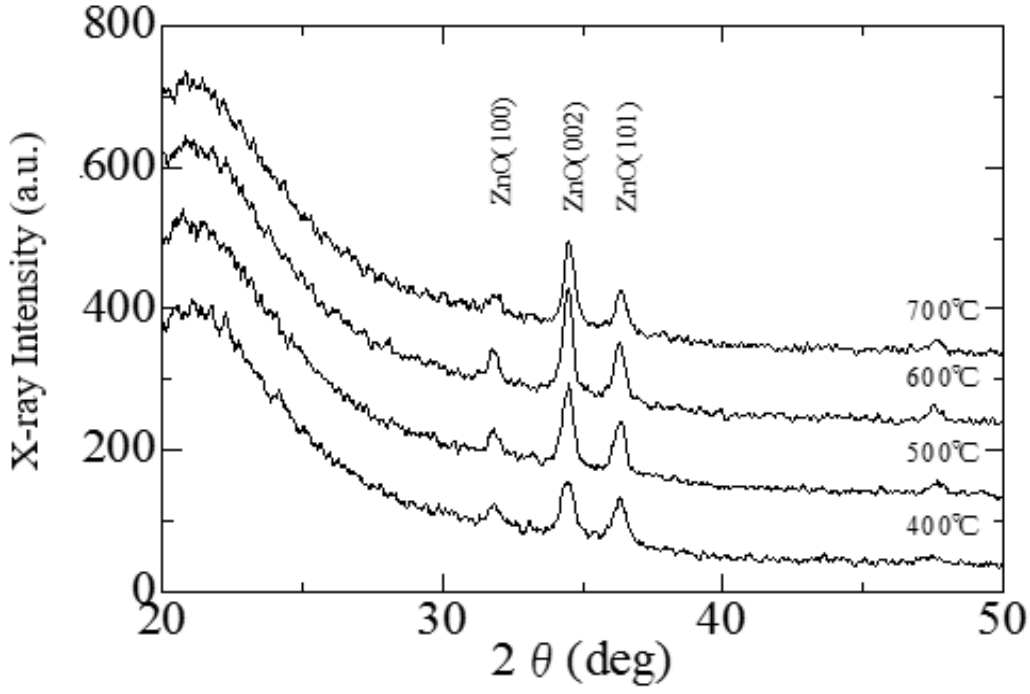

(b) Air

Figure 3.1. XRD spectra of the ZnO films deposited on quartz substrates and annealed under (a) Oxygen, (b) Air.

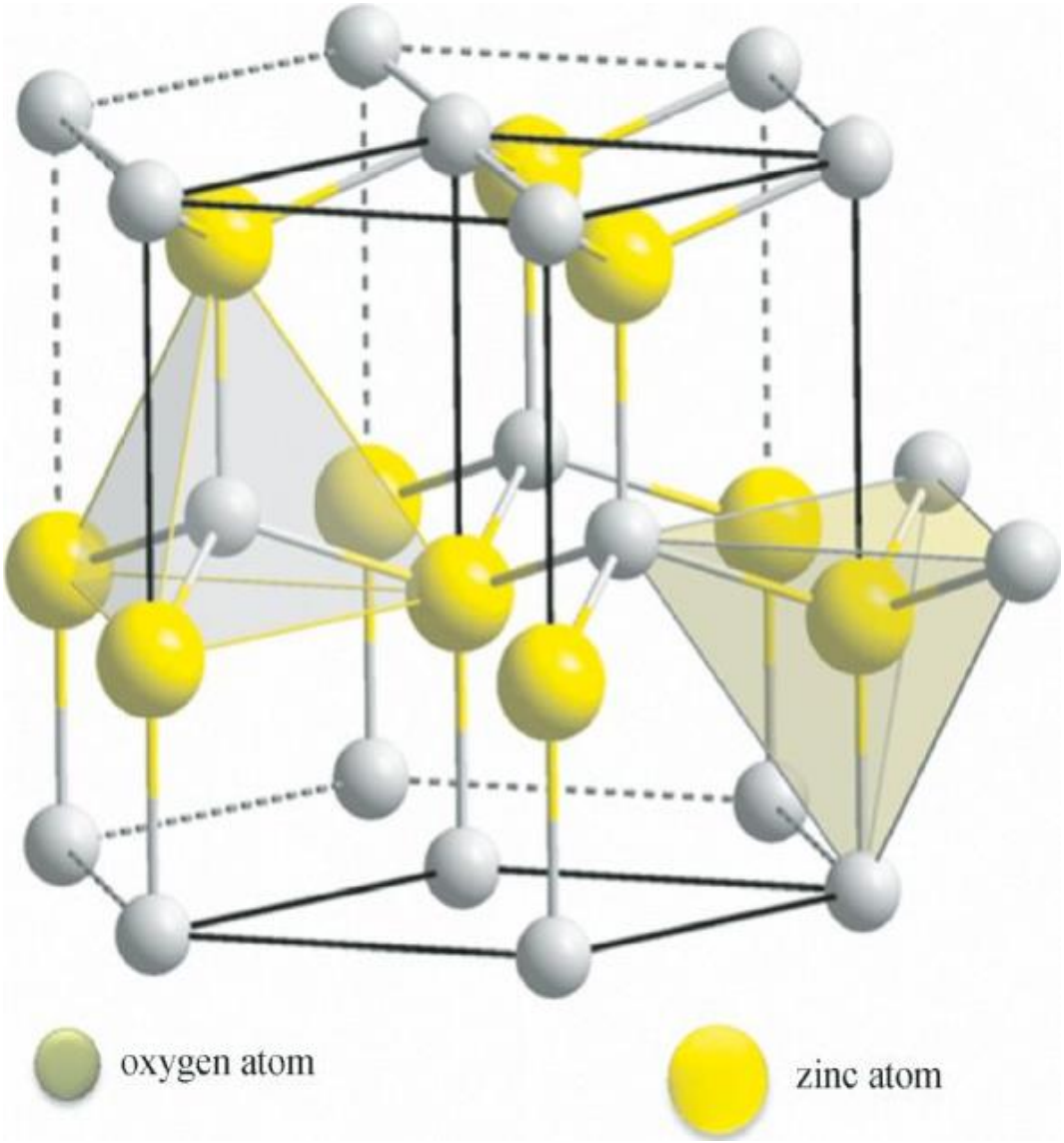

Figure 3.2. The wurtzite structure of ZnO films [52].

I measured the thickness of ZnO films by a film thickness monitor produced by Otsuka Electronics Co., Ltd, named FE-3000. The thickness of all ZnO thin films is shown in Figure 3.3. It is found that prior to annealing ZnO film thickness was 177 nm and annealing under atmosphere yielded smaller thicknesses. The thickness of annealed ZnO films fell as the annealing temperature rose. It is because more of the solvent evaporated at higher temperatures.

As two films that have different thickness can't be compared to each other in normalization, since the thicker the film is, the higher the peak's intensity is, I developed a new concept in crystallization study, which is called "Normalized X-ray Intensity". This metric is calculated by Equation 3.1.

$$X' = \frac{x}{d} \times 100 \qquad (3.1)$$

where *X*' is the normalized X-ray intensity, *X* is the measured X-ray intensity, and *d* is the film thickness. The annealing temperature dependence of the normalized X-ray intensities for ZnO (002) plane peak is shown in Figure 3.4. It seems that the normalized X-ray intensity rises with the annealing temperature, which means that the crystallization of ZnO films deposited by spin-coating method advances as the annealing temperature is raised.

Figure 3.5 shows the relationship between grain size and annealing temperature. The grain size was calculated by Scherrer's equation (Equation 3.2) [53].

$$D = \frac{0.9\lambda}{\beta \cos\theta} \qquad (3.2)$$

where *D* is the grain size (nm), λ is the wavelength of the incident X-ray, β is the full width at half maximum of the peak and θ is the center angle of the peak. In Figure 3.5, we find that the grain size increased with annealing temperature from 400 ℃ to 700 ℃, which matches the normalized X-ray intensity data. The crystallization of ZnO films deposited by the spin-coating method and then annealed has been proved

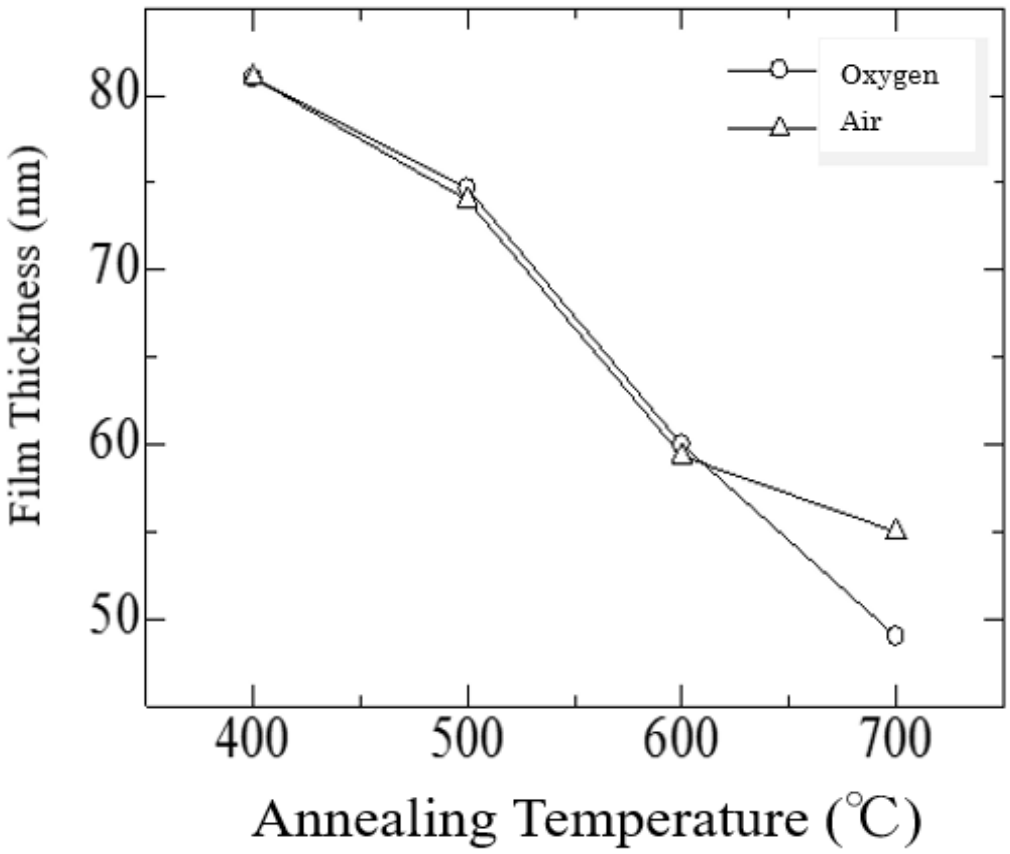

Figure 3.3. The relationship between the films' thickness and the annealing temperature.

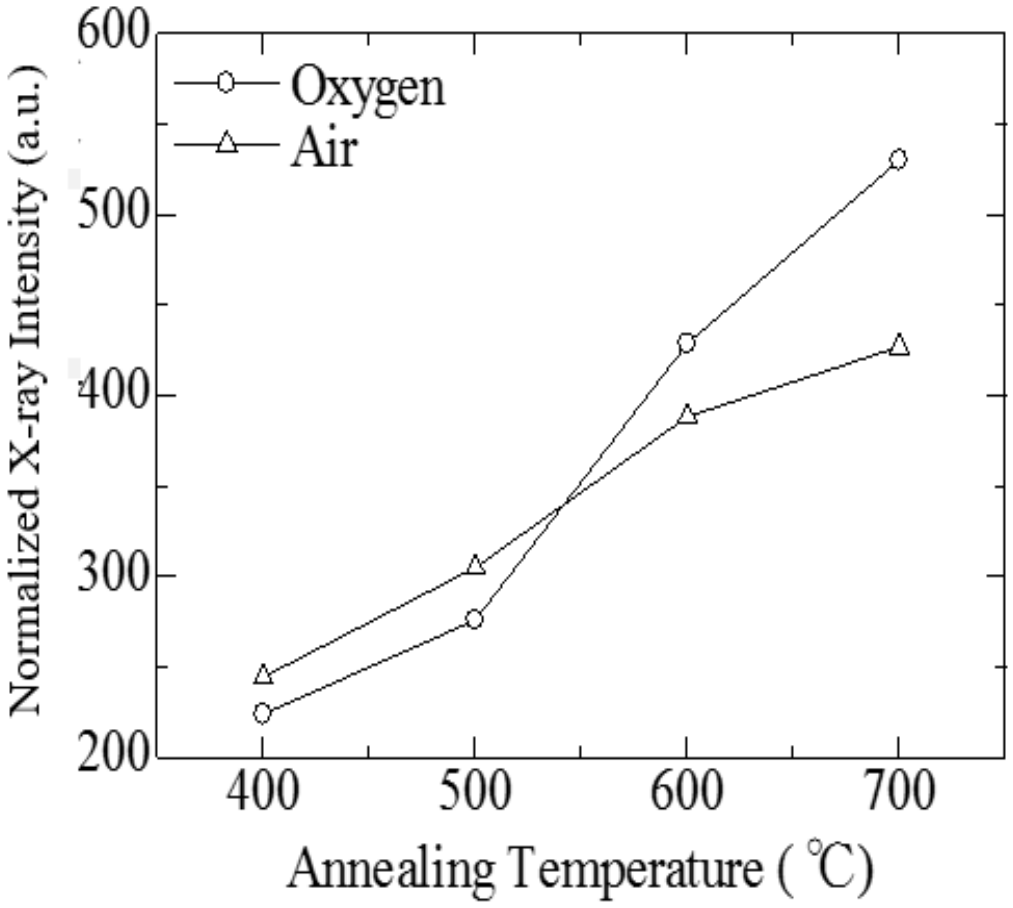

Figure 3.4. Annealing temperature dependence of the normalized X-ray intensities for ZnO (002) plane peak of ZnO films.

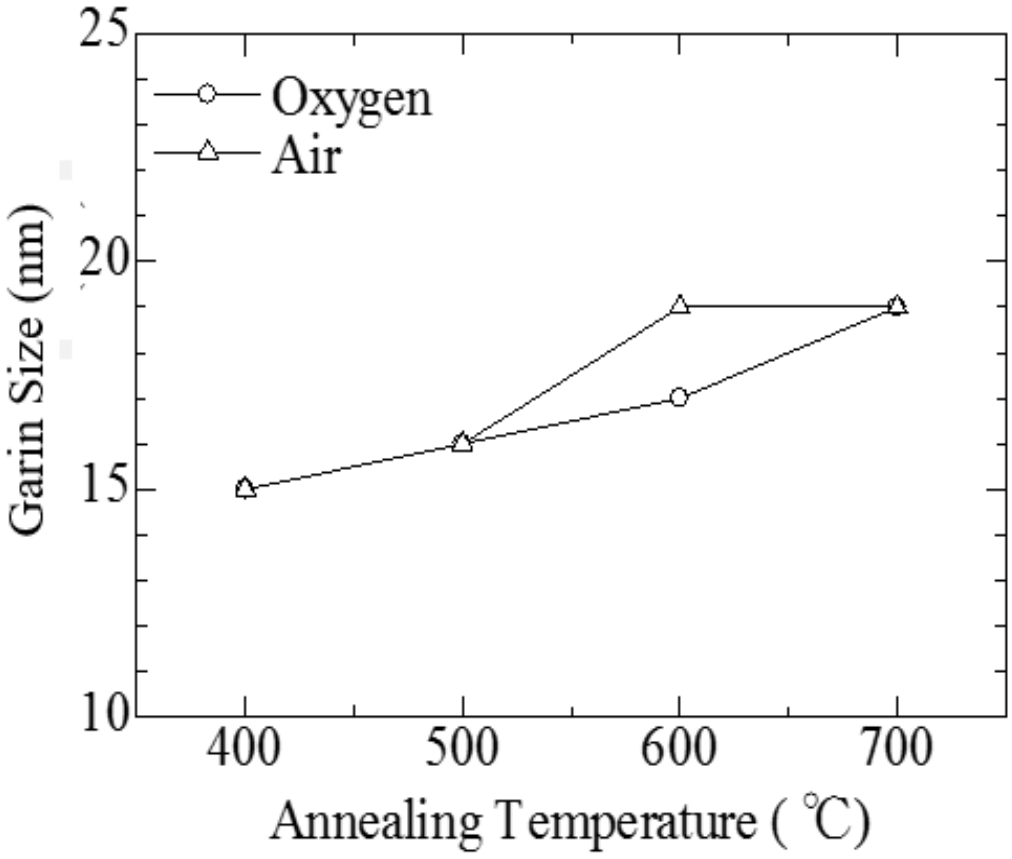

Figure 3.5. The relationship between the grain size and the annealing temperature of ZnO films.

again.

The average optical transmittance of all films is shown in Figure 3.6. The transmittance spectrum of ZnO films was measured for wavelengths from 400nm to 800nm. The optical transmittance is about 80%~90% in the visible range. It is found that the average optical transmittance of all films decreased as annealing temperature rose. Since the optical transmittance is dependent on film thickness, as is the normalized X-ray intensity, I developed the new concept in optical property called "Normalized Optical Transmittance". The normalized optical transmittance is calculated by Lambert-Beer Law (Equation 3.3) [54].

$$A = -\ln\frac{K}{K_o} = \varepsilon \mathrm{CL} \qquad (3.3)$$

where A is the absorbance, K is the intensity of the transmitted light, K_o is the intensity of the incident light, ε is the mole absorbance coefficient, C is the mole concentration, and L is the length of the light path. From Equation 3.3, we obtain Equation 3.4.

$$-\ln\frac{T}{100} = \varepsilon \mathrm{Cd} \qquad (3.4)$$

where d is film thickness, and

$$T' = 10^{\frac{100\times\ln\frac{T}{100}}{d}} \times 100 \qquad (3.5)$$

where T' is the normalized transmittance. As shown by Equation 3.5, this study assumes, for assessing normalized transmittance, that film thickness is 100nm. The normalized optical transmittance of all ZnO films is shown in Figure 3.7. It is found that the normalized optical transmittance decreased as annealing temperature was increased from 400 ℃ to 700 ℃. Maximum normalized transmittance of around 85% was observed for the ZnO films annealed at 400 ℃ in air.

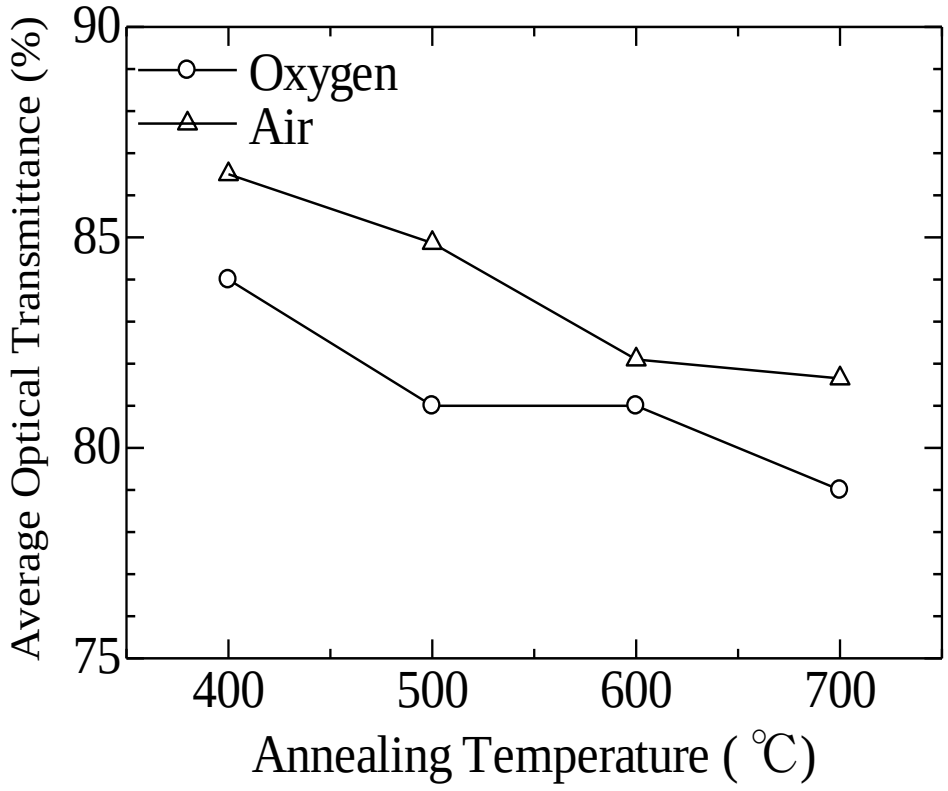

Figure 3.6. The relationship between the average optical transmittance and the annealing temperature.

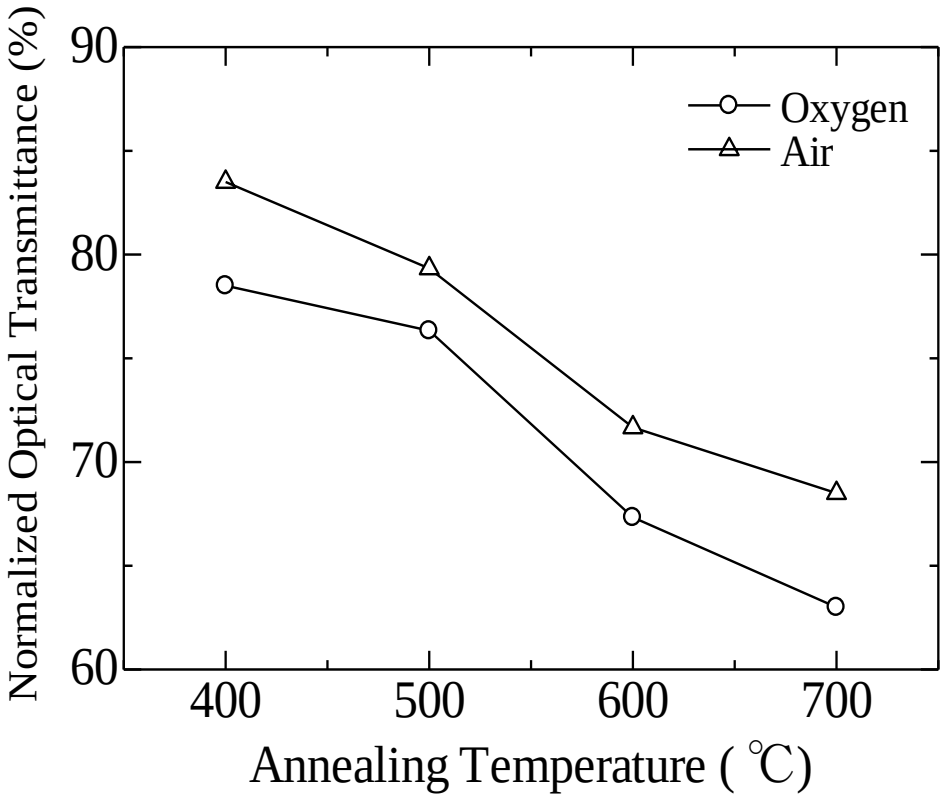

Figure 3.7. The relationship between the normalized optical transmittance and the annealing temperature of ZnO films.

Finally, I analyzed the electrical properties of ZnO films. At first, I tried to use the four probe position method, which is the most widely used technique to analyze the TCO film's electrical properties. Unfortunately, the resistivity values of the ZnO films deposited by the spin-coating method were too high to measure. I then applied a more complicated method but still failed to measure their resistivity. Thus the electrical properties of spin-coated ZnO films could not be analyzed.

As Transparent Conductive Oxide applications demand low resistivity, the spin-coating method failed to realize useful ZnO films. In order to overcome this difficulty, I turned my attention to Al-doped ZnO (AZO) films.

3.2 Effect on AZO Films

AZO films, in which the ZnO films are doped by Al, have good electrical and optical properties for transparent conductor applications, and Al is a cheap, abundant and non-toxic material. Therefore, AZO is an attractive candidate to replace ITO. In this experiment, I used the AZO solvent produced by KOJUNDO CHEMICAL LABORATORY CO., LTD. The Al/Zn atomic ratio in this solvent is 1/50. The deposited films were annealed at 400, 500, 600, or 700℃ in an electric furnace for 60 minutes under an atmosphere of oxygen or air. The same coating process was repeated for 9 times to obtain uniform thick films.

Figures 3.8(a) and 3.8(b) show the XRD spectra of the AZO films deposited on quartz substrates and annealed in oxygen and air, respectively. The XRD spectra show three pronounced diffraction peaks at 2θ=31.72, 34.45, and 36.21° positions; these peaks correspond to the ZnO planes of (100), (002) and (100), respectively. It is found that all of the annealed films showed strong peaks that correspond to their (002) preferred orientation. The intensity of the main peak corresponding to the (002) direction increased as the annealing temperature increased. Figure 3.9 shows the annealing temperature dependence of the normalized X-ray intensities for ZnO (002) peaks. The thickness of all AZO films is summarized in Table 3.1. The intensities for the films annealed in air were smaller than those annealed in oxygen. The normalized X-ray intensities increased as the annealing temperature increased, which is the same as in the ZnO measurements.

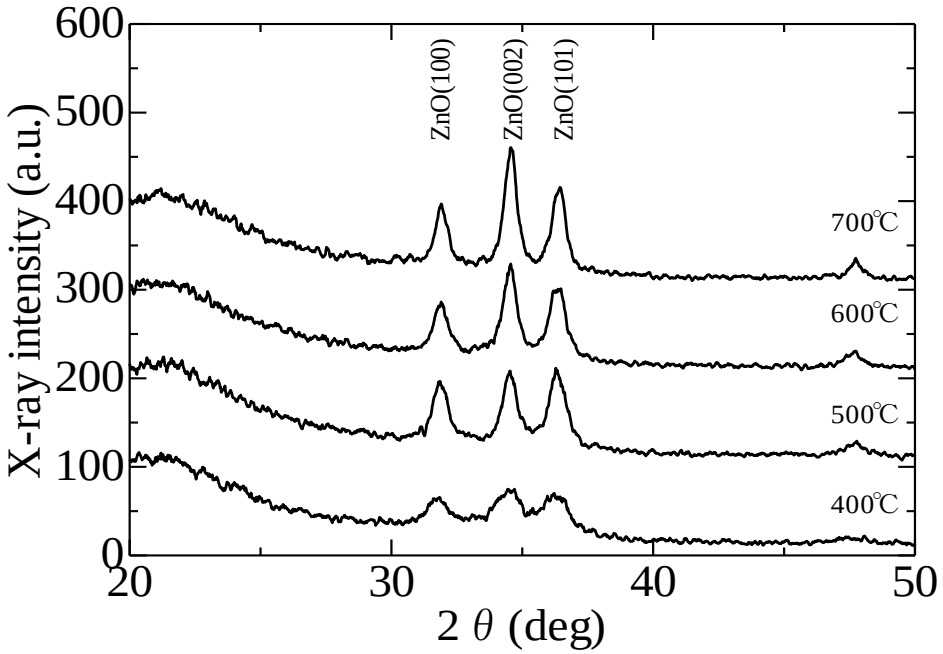

(a) Oxygen

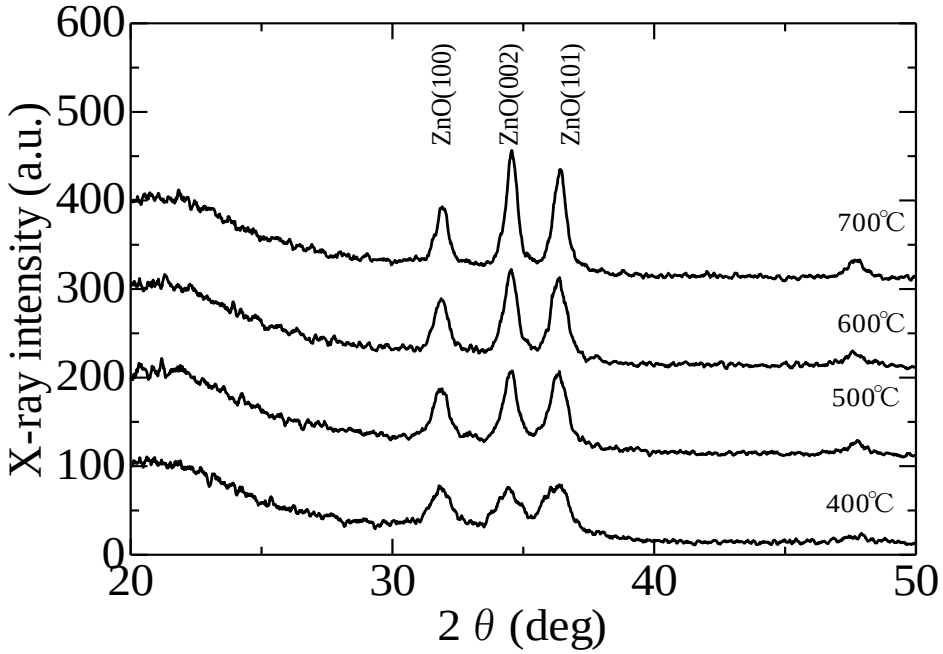

(b) Air

Figure 3.8. XRD spectra of the AZO films deposited on quartz substrates and annealed under (a) Oxygen, (b) Air.

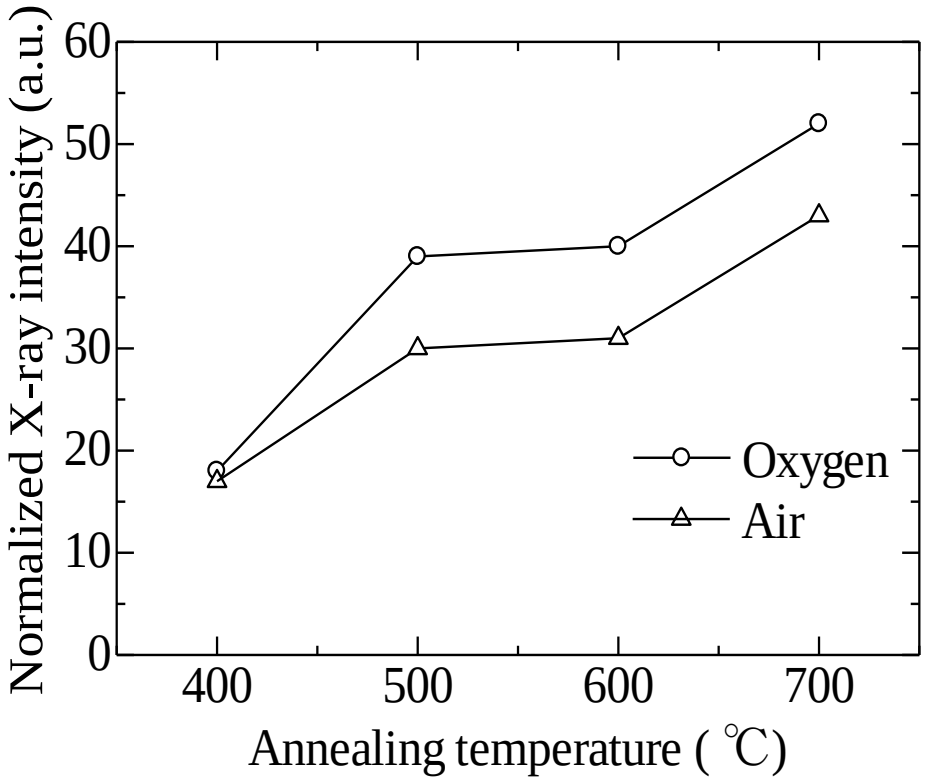

Figure 3.9. Annealing temperature dependence of the normalized X-ray intensities for ZnO (002) plane peak of AZO films.

Table 3.1. Thickness of the AZO films prepared by using spin-coating method.

Annealing temperature (°C)	**Film thickness (nm)**	
	Annealing ambient	
	Oxygen	Air
400	186	155
500	119	137
600	152	177
700	129	148

This suggests that the amount of Al dopant was too small to influence the ZnO films' structure.

Figure 3.10 shows the relationship between grain size and annealing temperature. In Figure. 3.10, it is found that the grain size increased with annealing temperature from 400°C to 700°C. The increase in grain size with annealing temperature is supported by the increase in normalized X-ray intensity from 400°C to 600°C, therefore, the higher the normalized X-ray intensity is, the larger grain size is. Upon comparing the grain size of ZnO films and AZO films, I found that, for the same annealing conditions, AZO films had smaller grain size than ZnO films. This is because Al ions have smaller radius (0.0535nm) than Zn ion (0.074nm), and Al ions replaced some of the Zn ions in the deposition process [55].

Figure 3.11 depicts the variation of resistivity (ρ) of Al-doped ZnO films with annealing temperature. The resistivity first decreased as annealing temperature increased from 400°C to 500°C and the lowest resistivity (1.01Ωcm for the film annealed in oxygen and 1.4Ωcm in air) was obtained at the annealing temperature of 500°C. With further increase in annealing temperature, the resistivity started to increase significantly. The decrease in resistivity as annealing temperature increased from 400°C to 500°C can be attributed to an increase in the grain size of the AZO thin films from 11 nm to 23 nm for the film annealed in oxygen and 14 nm to 21 nm in air, therefore, increasing the crystallite size of AZO thin films can decrease grain boundary scattering and increase the carrier lifetime which yields lower resistivity. However, the resistivity increased as annealing temperature rose from 500°C to 700 °C. It has been reported that high annealing temperatures results in higher resistivity due to defect association [56].

Figure 3.12 shows the relationship between the normalized optical transmittance and the annealing temperature. The transmittance spectrum of AZO films was measured for wavelengths from 400 nm to 700 nm. The optical transmittance was about 85 to 95% in the visible range. The normalized optical transmittance decreased as annealing temperature rose from 400°C to 700°C. Maximum normalized transmittance of around 92.1% was observed for the AZO films annealed at 400°C in oxygen.

Since ZnO film is a direct transition semiconductor, Equations 3.6 and 3.7 were used to calculate the optical band-gap of all films [57].

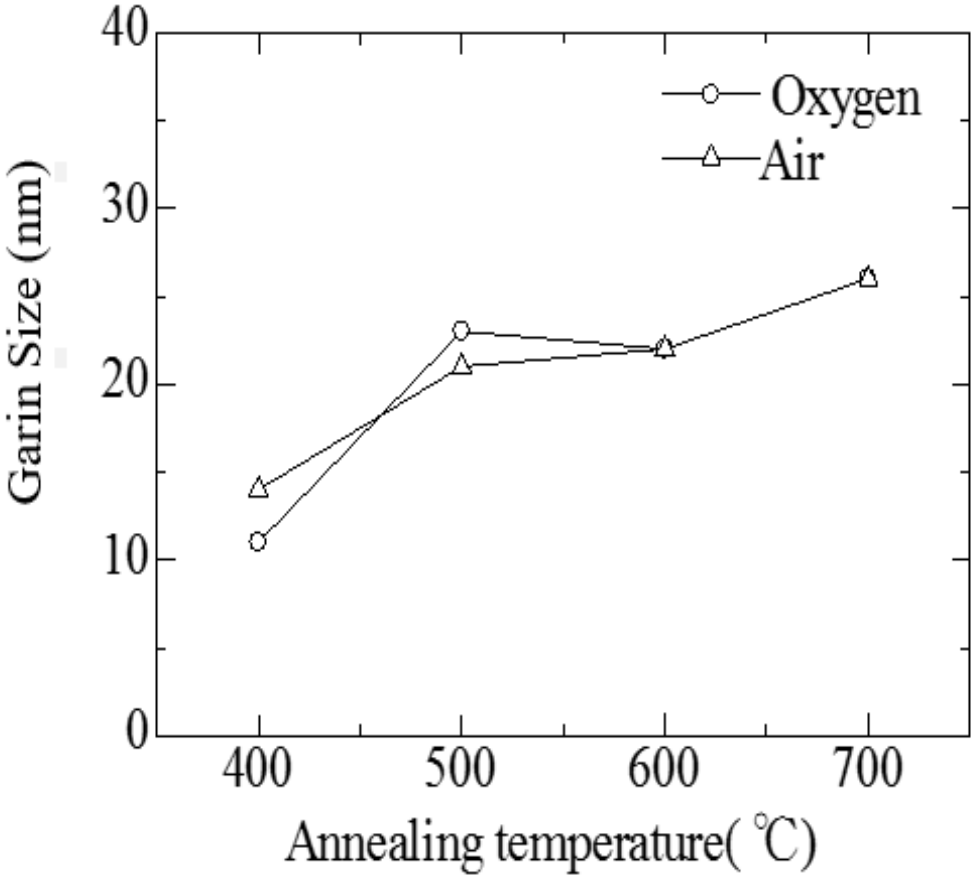

Figure 3.10. The relationship between the grain size and the annealing temperature of AZO films.

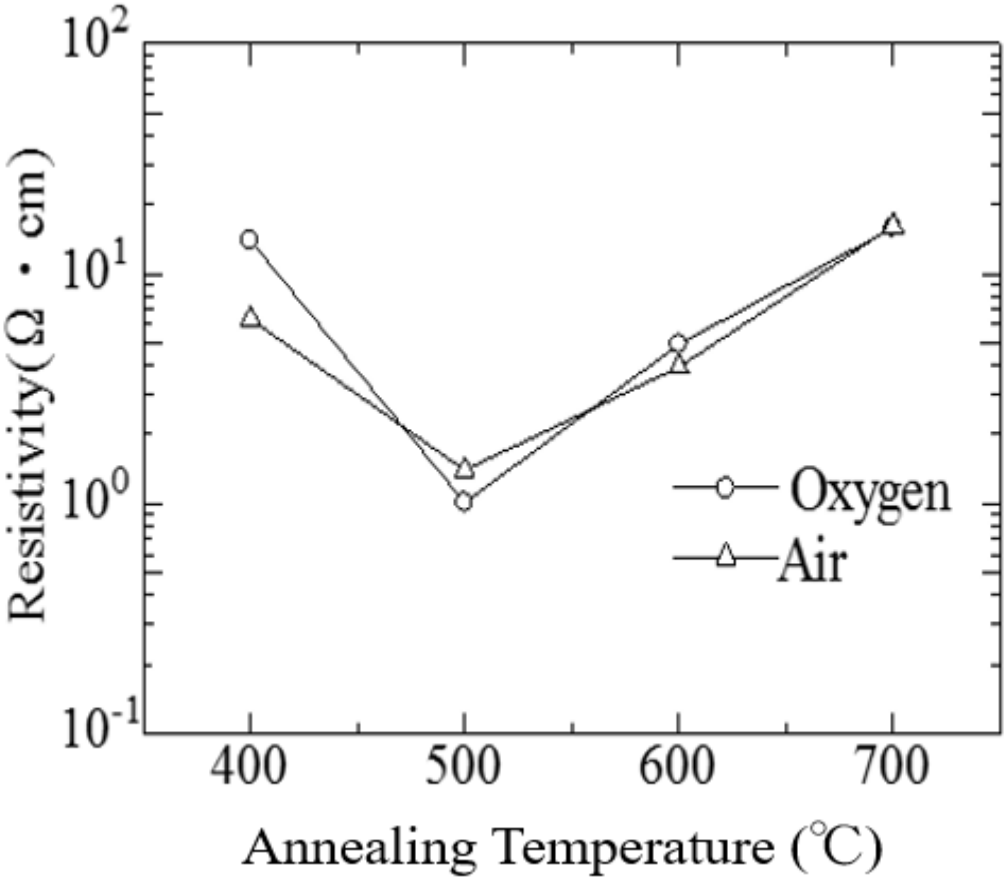

Figure 3.11. Relationship between resistivity and annealing temperature of AZO films.

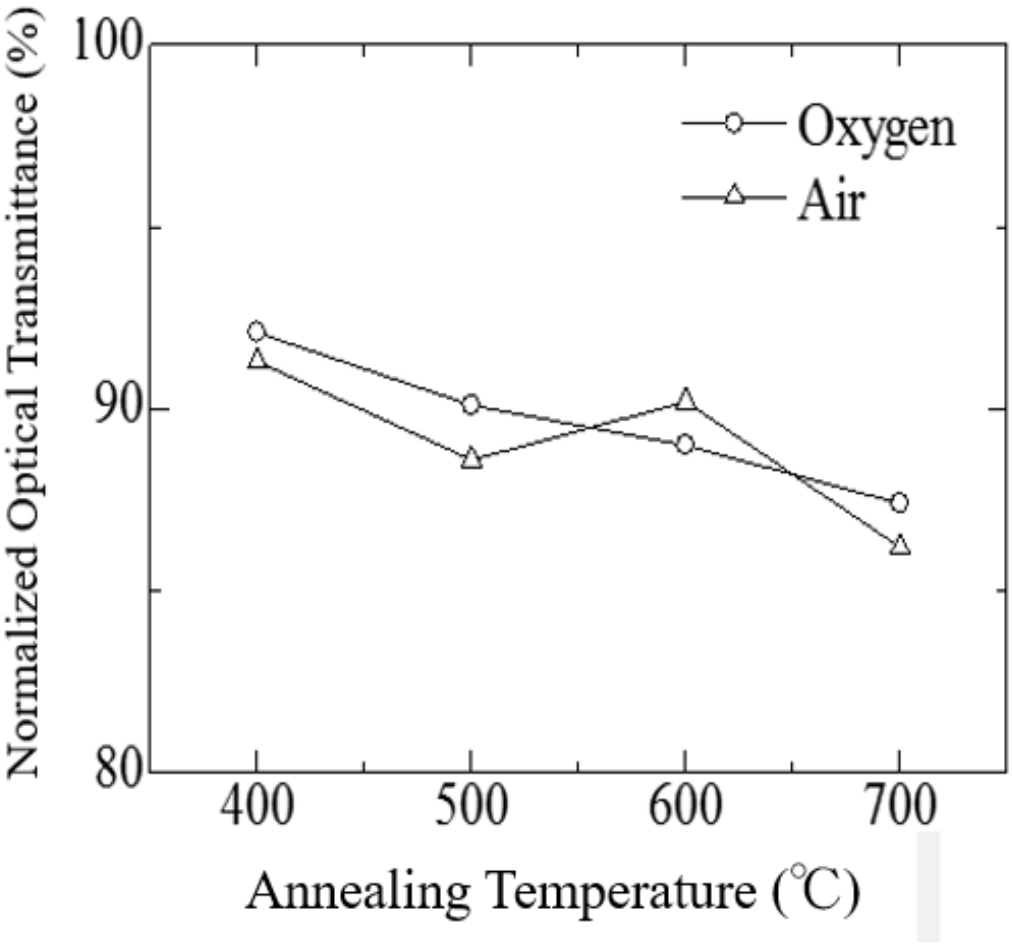

Figure 3.12. The relationship between the normalized optical transmittance and the annealing temperature of AZO films.

$$(\alpha h\nu)^2 = A(h\nu) - \mathrm{E_g} \tag{3.6}$$

$$\left(1/d\right)^2 \ln^2\left(1/\mathrm{T}\right)\left(\frac{hc}{\lambda}\right)^2 = \mathrm{A}\left(\frac{hc}{\lambda} - \mathrm{E_g}\right) \tag{3.7}$$

where A is the coefficient of direct transition, ν is photon frequency and the λ is the wavelength.

$$\frac{(\alpha h\nu)^2}{h\nu} = \left(1/d\right)^2 \ln^2\left(1/\mathrm{T}\right)(h\nu) \tag{3.8}$$

Figure 3.13 shows the optical band-gap of the ZnO films and AZO films deposited by using the spin-coating method. The figure shows that for the same annealing conditions, AZO films have higher optical band-gap than ZnO films. It is because as the doping concentration is increased, electrons populate states within the conduction band which pushes the Fermi level higher in energy and in the case of degenerate level of doping, the Fermi level lies inside the conduction band. In this case, an electron from the top of the valence band can only be excited into the conduction band above the Fermi level (which now lies in conduction band) since all the states below the Fermi level are occupied states. Pauli's exclusion principle forbids excitation into these occupied states. Thus an increase in the apparent band gap is observed. Apparent band gap is given by E_g+ ΔE as shown in Figure3.14 [58].

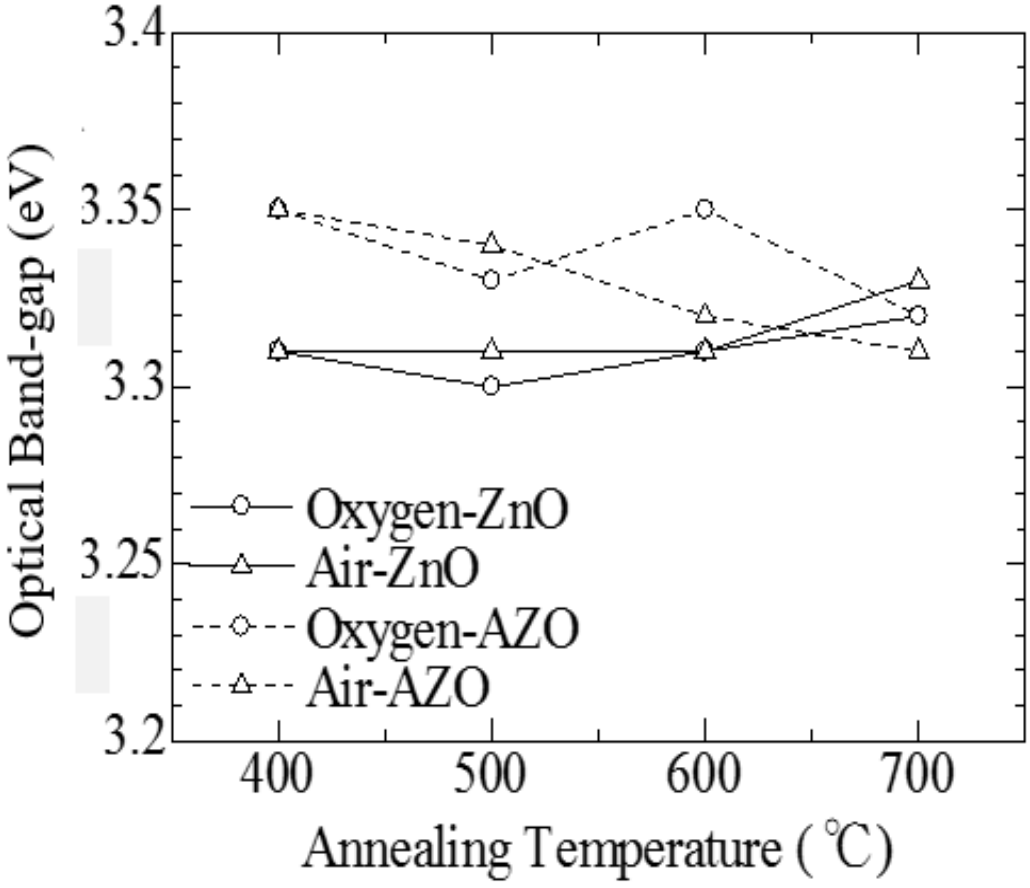

Figure 3.13. The relationship between the optical band-gap and annealing temperature of ZnO films and AZO films.

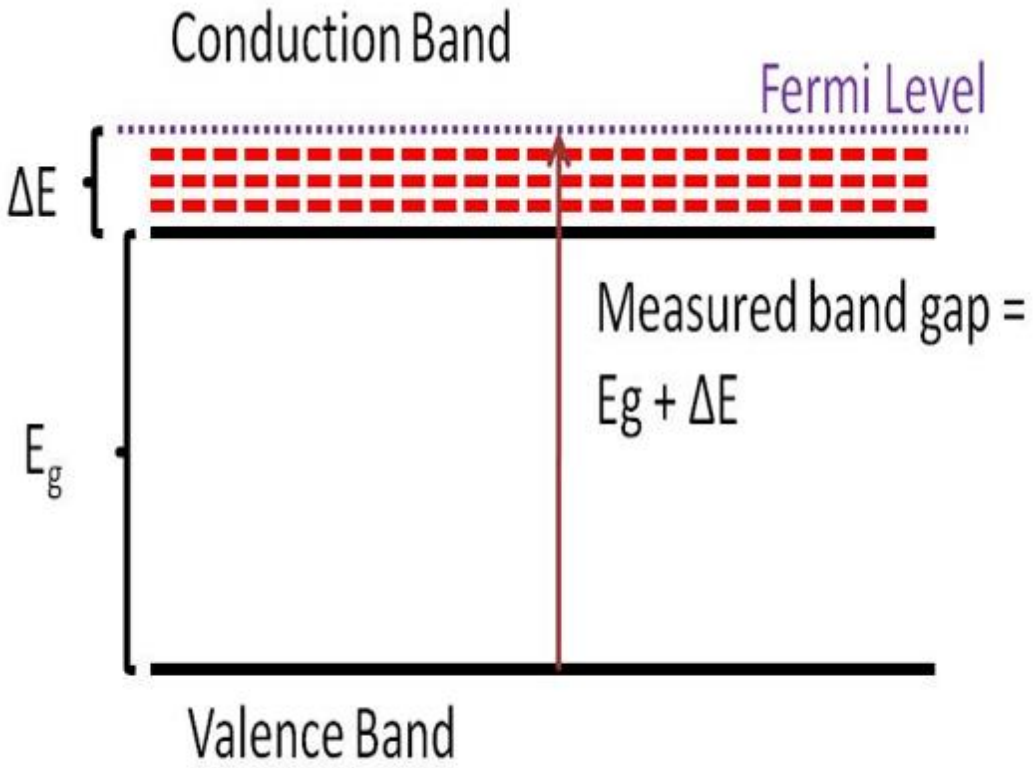

Figure 3.14. The reason of the increment in optical band-gap [58].

Chapter 4. THE ELECTRICAL TRANSPORT PROPERTY OF ZnO THIN FILMS BY RADIO FRERQUENCY SPUTTERING METHOD

4.1 Introduction

This Chapter discusses the electrical property of ZnO films deposited by using the RF sputtering method. In the previous Chapter, I found that the resistivity of ZnO and AZO films deposited by using the Spin-coating method is so high that the films are not suitable for TCO applications. This triggered the desire to elucidate the fundamental mechanism of carrier (electron) generation of ZnO films with the goal being the lowest resistivity. Since ZnO films deposited by the Spin-coating method have a non-uniform surface, I turned to the more sophisticated RF sputtering method to create more uniform ZnO films.

Since thin ZnO films have, generally speaking, a poly-crystalline structure, it is anticipated that grain boundary scattering is dominant factor determining electrical transport [59]. It is considered, based on many experiments, that electron generation in undoped ZnO thin films is due to the oxygen vacancies (Vo) created by ZnO bonding [60] because undoped ZnO films are generally n-type semiconductors, and/or intrinsic donors due to the interstitial Zn atoms (Zn_i) [61]. Note that oxygen vacancies (Vo) and zinc interstitial Zn_i in ZnO have low formation energies. However, these low-energy intrinsic defects could also be responsible for the equilibrium p-type doping difficulties of ZnO [62]. An experiment has shown that the electron concentration is much higher than the concentration of ionized oxygen vacancies [63]. In addition, recent theoretical simulations have predicted that oxygen vacancies (Vo) yield deep states in the band gap [64], while interstitial Zn atoms (Zn_i) do not always play the role of potential donors [64,65]; it has been suggested that hydrogen-related donors are responsible for electron generation [64,66].

As the primary aim of this work is to elucidate the dominant mechanism controlling the electrical property of undoped ZnO films and impurity-doped ZnO films, we must clearly identify the structural aspects of undoped ZnO films. In some cases, I regard the measured chemical and physical properties of ZnO as only

rough estimates, not as highly reliable values. Since the characteristics of ZnO films are expected to be dependent on fabrication conditions, I carefully investigated the various factors that may modify the structure and property of ZnO films.

To this end, I characterized the oxygen bonding state by X-ray photoelectron spectroscopy (XPS). I propose an advanced method to characterize the relation between the oxygen-related spectrum component and the electron concentration. The relation between oxygen-bonding states and oxygen vacancy generation is discussed from various viewpoints of the films' electrical properties. In addition, I trace the evolution of the in-depth concentration profile of oxygen isotope atoms that are captured by the ZnO films during deposition in order to elucidate how oxygen atoms and oxygen vacancies behave and contribute to electron generation. I reveal how the annealing condition after deposition changes the in-depth profile of oxygen atoms.

4.2 Experiments

The sample deposition process was described in Chapter 2.2, and the structure of samples used to characterize the electrical properties overviewed in Fig. 2.4. For the physical and chemical analyses, the crystalline orientation and the grain size of several ZnO films were characterized by an X-ray diffractometer using CuK_{α} radiation at the excitation voltage of 50 kV and current of 300 mA. The atomic composition of the films was measured by the Rutherford back-scattering (RBS) technique. In order to examine the electrical characteristics of deposited films, I measured the current vs. voltage (*I*-*V*) characteristics using Pt electrodes. Electron concentration of films annealed under nitrogen ambient was evaluated by the Hall effect at room temperature. Since the electron concentration of the films was not so high (shown later), I consider the measured values to be only rough values. In this experiment, we need the chemical bonding information of the deposited ZnO films in order to elucidate the origin of electron generation and the role of oxygen vacancy. X-ray photoelectron spectroscopy (XPS) was used to chemically analyze oxygen bonding states in the film. The XPS analyses used an Al $K_{\alpha 1,2}$ (1486.6eV) monochromatic X-ray source. I decomposed the O1s spectra to better understand the relation between oxygen vacancy concentration and electron concentration.

4.3 Results and discussion

4.3.1 Current - Voltage Characteristics

The current-voltage characteristics of four types of ZnO films at room temperature are shown in Figure 4.1. The first sample type, called “film A”, was deposited under pure argon and annealed under nitrogen. The second type, called “film B”, was deposited under pure argon and annealed under oxygen. The third type, called “film C”, was deposited under a mixture of argon and oxygen and annealed under nitrogen. The last type, called “film D”, was deposited under a mixture of argon and oxygen and annealed under oxygen. The deposition conditions and annealing conditions are summarized in Table 4.1.

From Figure 4.1, I find that all four types of samples exhibit ohmic conduction in the voltage range of 0.01 V to 0.1 V although the two annealed under oxygen ambient reveal sub-linear or saturation current behavior at voltages higher than 0.1 V. As seen in Figure 4.1, the lateral resistances of films A and C, annealed under nitrogen gas, are much lower than those of films B and D, annealed under oxygen gas. In addition, the lateral resistance of film A is much lower than that of film C. In contrast to the films annealed under nitrogen ambient, the lateral resistance of film B (deposited under Ar gas) is higher than that of film D (deposited under a mixture of Ar gas and oxygen gas and annealed under oxygen ambient).

Next, I used Hall effect measurements to evaluate the electron concentration of every film. The Hall-effect measurements revealed that the primary carriers ruling conduction are electrons, so all 4 types of ZnO films are n-type semiconductors. As was mentioned previously, I don’t take these measured values as highly reliable. I show the relation between electron concentration and fabrication conditions in Figure 4.2. The horizontal axis plots the ambient gas conditions; for example, Ar-N_2 means that the film was deposited under Ar gas and annealed under N_2 gas. The results suggest that the films annealed under N_2 gas have much higher electron concentrations than the films annealed under O_2 gas regardless of the deposition ambient gas.

As seen in Figure 4.1, films A and C (annealed under nitrogen ambient) clearly show ohmic conduction even at 5 V (~10^2 V/cm), which suggests that the electrical measurements are successful and that the films are semiconductors. As a result, the electron concentration values estimated by the Hall effect are reliable in a

Table 4.1. Film deposition conditions and anneal conditions.

Samples	Deposition			Annealing		
	RF power density (W/cm^2)	Gas	Pressure (Pa)	Gas	Temperature (℃)	Time (min.)
A	1.99	Ar(100%)	0.66	N_2	700	10,30,60
B				O_2		
C		Ar/O2 (50%/50%)		N_2		
D				O_2		

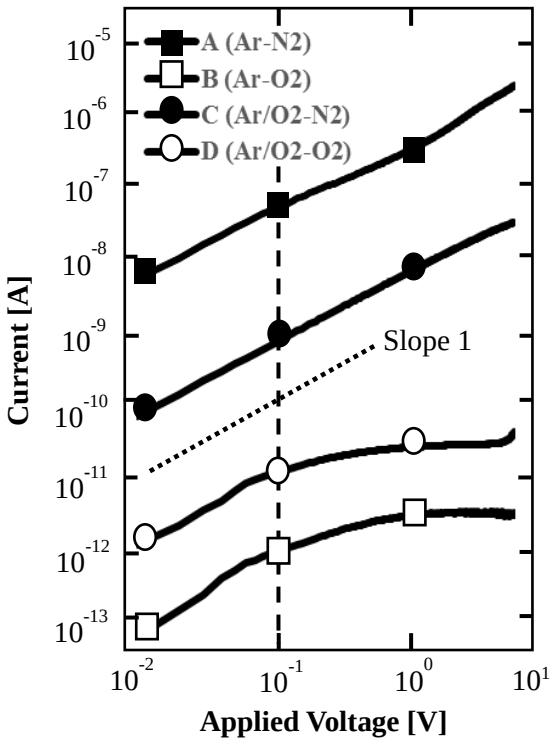

Figure 4.1. Current – voltage characteristics of four different ZnO films. All films were annealed for 60 min.

Films A and C exhibit ohmic conduction.

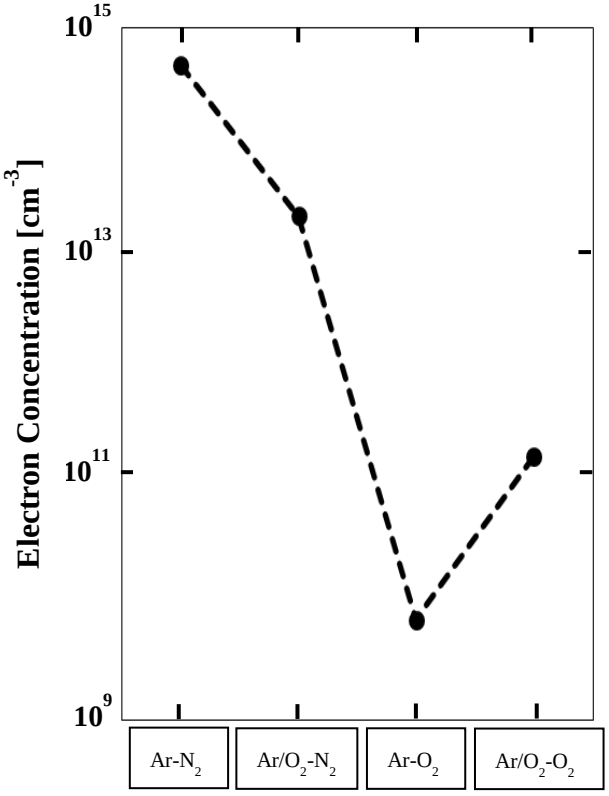

Figure 4.2. Electron concentrations of films deposited and annealed under various ambient gas conditions. The electron concentrations are obtained by the Hall effect at room temperature. All films were annealed for 60 min.

semi-quantitatively manner. On the other hand, films B and D (annealed with the oxygen ambient) show non-ohmic conduction in a high-voltage range (see Figure 4.1), which suggests that the films should be dielectrics rather than semiconductors. Therefore, except for the XPS analyses, I focused on the characteristics of films A and C.

As evidenced by recent studies, the physical and optical properties of ZnO nanowires are the center of attention in a number of emerging areas such as low-voltage and short-wavelength optoelectronics [67]. However, such properties are more sensitive to fabrication process conditions than ZnO films due to the small dimensions involved [68,69]. As the physical and optical properties of thin films are averaged across the plane, it is anticipated that stable properties can be obtained.

4.3.2 X-ray Diffraction Results

The crystalline structures of the ZnO films were identified by X-ray diffraction (XRD). The diffraction data of the ZnO films deposited and annealed under the different ambient gas conditions are shown in Figure 4.3; a specific peak is observed around 34.5 deg for the ZnO (002) plane. The XRD results show that, like the ZnO films deposited by using spin-coating method, all as-prepared films are polycrystalline with preferred orientation along the ZnO (002) plane, which suggests that all films have the hexagonal wurtzite structure.

The crystallite size of the ZnO films was determined using Scherrer's formula,

$$D = 0.9\,\lambda/\beta\cos\theta, \qquad (4.1)$$

where D is grain size (nm), λ is the wavelength of the incident X-ray, θ is the center angle of the peak, and β is the full width at half maximum of the peak. In this study, I assume $\beta = [\beta_e^2 - \beta_0^2]^{1/2}$, where β_e is half-value width and β_o is the corrected value (3°). The values of 2θ, half-value width, and grain size are summarized in Table 4.2. The grain size of the films varies from 10 to 12 nm. It should be noted that films A and C, annealed under nitrogen gas, have almost the same grain size as films B and D, annealed under oxygen gas. It has been suggested that the lateral transport property of polycrystalline ZnO film is dominated by grain boundary

Table 4.2. XRD results (crystallite size) for various ZnO films.

Film Category	Gas (Depo.-Anneal)	2θ [deg.]	Half-value width [deg.]	Grain size [nm]
A	Ar-N_2	34.54	0.754	12.0
C	Ar/O_2-N_2	34.56	0.804	11.2
B	Ar-O_2	34.65	0.835	10.7
D	Ar/O_2-O_2	34.64	0.884	10.0

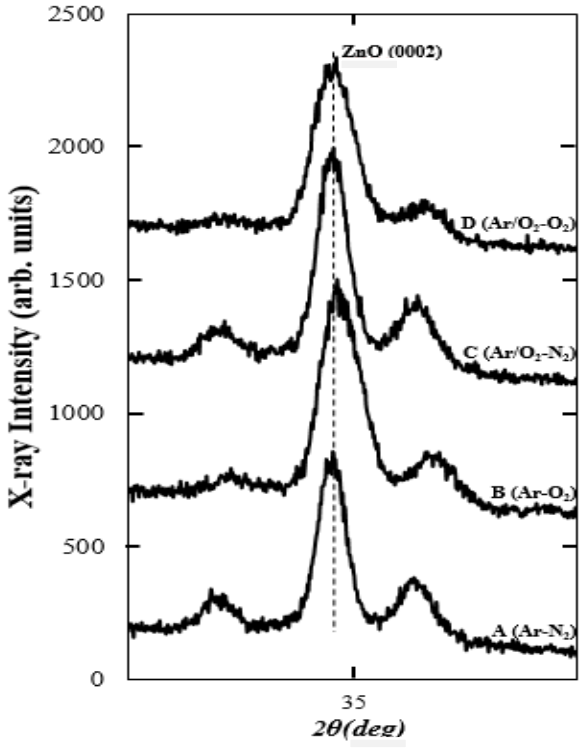

Figure 4.3. X-ray diffraction curves for various ZnO films. All films were annealed for 60 min.

scattering [70]. Accordingly, I tentatively assume that grain boundary scattering makes a similar contribution to the electrical transport properties of the ZnO films examined here.

4.3.3 Rutherford Back Scattering Analysis

Figure 4.4 shows an example of the in-depth profiles of the normalized atomic ratio values of the ZnO films (film B) deposited under Ar gas and annealed under O_2 ambient. The atomic ratios of various ZnO films are summarized in Table 4.3. We can see that the ZnO films deposited or annealed under oxygen ambient have higher oxygen atomic ratios than those deposited or annealed under oxygen-free ambient. This suggests that oxygen ions can diffuse deeply into the ZnO films when the films are deposited or annealed under an ambient containing oxygen.

4.3.4 X-ray Photoelectron Spectroscopy

XPS spectra are widely used to identify the chemical bonding states and to analyze the bonding energy variation in thin films [71]. Figure 4.5 shows the XPS spectra of a ZnO film (film A). Wide-scan spectra are shown in Figure 4.5(a) and narrow-scan spectra around the O1s-related components are shown in Figure 4.5(b).

I confirmed that there are no observable shifts in Zn-related or O-related primary spectra in response to the deposition condition or annealing condition. Peaks located at 1022 eV and 1045 eV correspond to the chemical states of $Zn2p_{3/2}$ and $Zn2p_{1/2}$, respectively; this indicates that the Zn ions mainly have the 2^+ state [72]. It is clearly seen in Figure 4.5(b) that the spectral profile of the O1s signal is not symmetrical, which suggests that the O1s spectrum consists of multiple spectra [73]. In Figure 4.5(b), the spectral profile of the O1s signal is decomposed into three possible components, which are examined later; the left spectra are obtained at the film surface and the right spectra are obtained in the film body region after Ar etching of the film. Though details of the XPS spectra are not shown in Figure 4.5(a), the surface of the post-annealed film was fatally contaminated by carbon compounds, which means that the XPS data at the surface are not reliable. Therefore, I dropped consideration of the data taken from the surface. The O1s spectra shown in the right side of Figure 4.5(b) are used in the following discussion.

Table 4.3. Atomic ratio in ZnO films

Film category	Gas (Depo-Anneal)	O/Zn atomic ratio
A	$Ar\text{-}N_2$	1.02
B	$Ar\text{-}O_2$	1.03
C	$Ar/O_2\text{-}N_2$	1.03
D	$Ar/O_2\text{-}O_2$	1.04

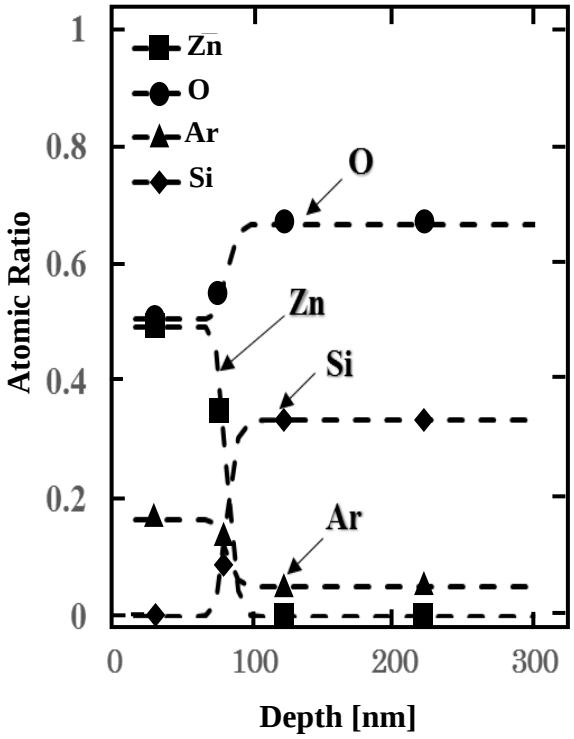

Figure 4.4 Example of in-depth atomic ratio profiles of sample (film A).
The film was annealed for 60 min.

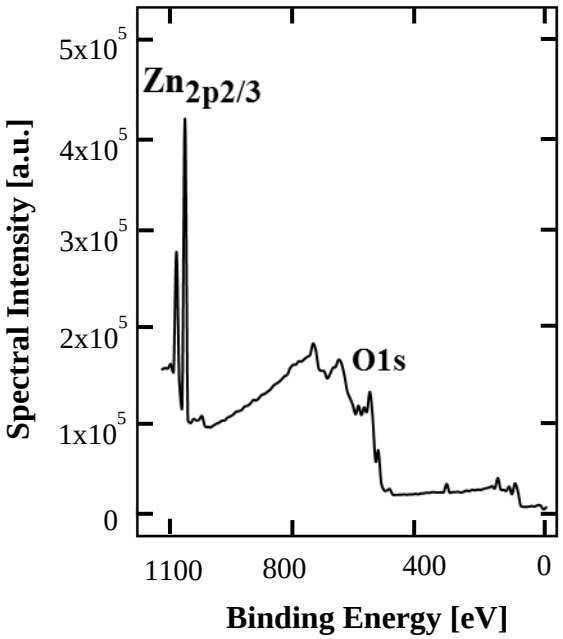
Zn2p2/3
O1s
Spectral Intensity [a.u.]
5x10^5
4x10^5
3x10^5
2x10^5
1x10^5
0
1100
800
400
0
Binding Energy [eV]

(a)

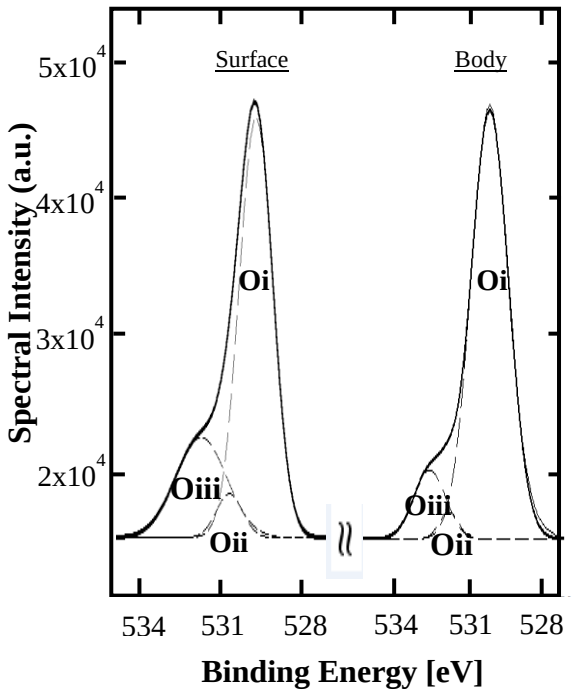
Surface
Body
Oi
Oi
Oiii
Oii
Oiii
Oii
Spectral Intensity (a.u.)
5x10^4
4x10^4
3x10^4
2x10^4
534
531
528
534
531
528
Binding Energy [eV]

(b)

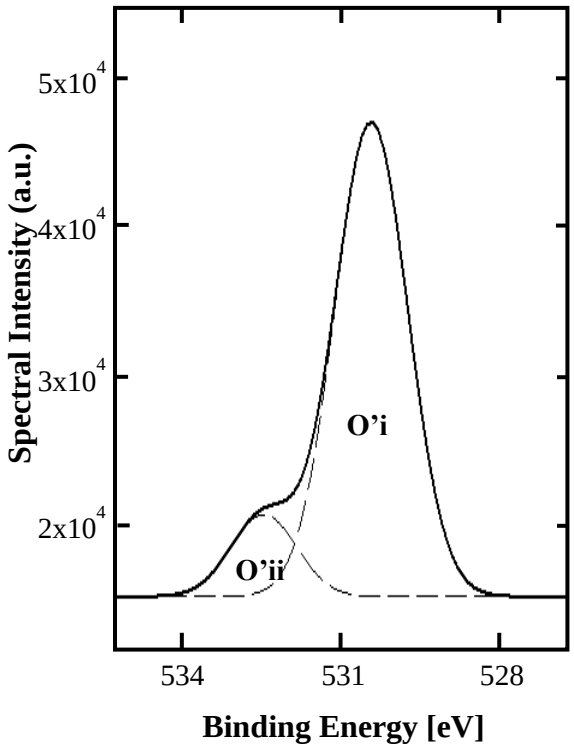

(C)

Fig. 4.5. X-ray photoelectron spectroscopy spectra of ZnO film (film A). The film was annealed for 60 min. (a) wide scan spectra, (b) narrow scan spectra around O1s spectra. The original O1s spectra are decomposed into 3 oxygen-related spectra. The left spectra are obtained at the film surface before Ar etching, and the right spectra are obtained in the film body after Ar etching. (c) narrow scan spectra around O1s spectra. The original O1s spectra are decomposed into 2 oxygen-related spectra.

Controversy surrounds the analysis of the O1s peak of ZnO films. Some studies [74,75] state that the spectral profile of the O1s signal can be decomposed into two spectra where the best fit to the asymmetric peak consists of two nearly Gaussian components, centered at 530.3eV (O'i) and 531.9eV (O'ii) (see Figure 4.5(c)); this is the conventional understanding. It has been considered that the O'i peak is attributed to the O^{2-} ions in the ZnO crystal lattice, and that the O'ii peak (so-called sub-peak spectrum) is attributed to the O-H bonds of the H_2O molecules absorbed by the films**.** In contrast to the conventional idea, other studies [76.77] state that the spectral profile of the O1s signal can be fitted by three Gaussian profiles as shown in Fig. 6(b), centered at 530.5 eV (Oi), 531.6 eV (Oii), and 532.6 eV (Oiii); it is assumed that the Oii spectrum lies between the Oi spectrum and the Oiii spectrum. I consider that this decomposition approach can reproduce the original O1s-related source spectra better than the conventional alternative. This approach is also applied to the analysis of TiO_2 films in recent studies [78, 79], where the interpretation of the three components is basically identical to that shown above. Therefore I apply this decomposition approach to the analysis of the XPS spectra.

The Oiii peak has a binding energy higher by about 2.1eV than that of the Oi peak. The lowest energy peak (Oi) corresponds to O-Zn bonding, and is attributed to oxygen ions neighboring Zn atoms that form the full complement of six nearest-neighboring oxygen ions. On the other hand, the highest energy peak (Oiii) is generally ascribed to chemisorbed oxygen ions at the grain boundaries or at the surface of the film. In addition, it is considered that the oxygen ions contributing to the generation of the Oiii spectrum lie in oxygen-deficient regions. The interpretation of the Oii peak (around 531.6 eV) remains controversial. Some studies [80, 81] report that the peak is associated with the O^{2-} anions in the matrix of the ZnO region, while other papers [82, 83] state that this peak develops with increasing loss of oxygen and so must be ascribed to oxygen vacancies (Vo).

In order to examine those predictions, I fabricated ZnO films with different annealing times (10, 30, and 60 min), and then applied the Ar etching technique to remove the films' surfaces since they are readily contaminated by moisture and other chemicals "present in the atmosphere prior to the annealing" during the annealing. The electron concentration of the films was also estimated by the Hall effect. Here I introduce an equation to examine the relative concentration of every atomic component [84].

$$G = h_G / [h_{Oi} + h_{Oii} + h_{Oiii} + h_{Zn2p}], \quad (4.2)$$

where G is the rate of any one of the denominator components, and h_G is the magnitude of any denominator component. Behavior of parameter h_G is summarized in Table 4.4.

I use the Gaussian fitting method to decompose the original spectral profile of the O1s signal two times. In the first step, I applied the conventional two-decomposition approach to the O1s source spectra in order to examine whether the conventional sub-peak spectrum (O'ii) yields a meaningful result. In the second step, I applied the three-decomposition approach [76, 77]. As it is considered that the electron generation of ZnO films is ruled by the generation of oxygen vacancies [85], I tried to verify the relationship between the proportion of O'ii peak intensity and the electron concentration (see Figure 4.6). It is seen that the film annealed for 30 minutes has the highest electron concentration, and that the film annealed for 10 minutes has a higher electron concentration than that annealed for 60 minutes. However, we can see that the proportion of the O'ii peak simply increases from 10 min to 60 min, which is inconsistent with the electron concentration behavior.

In Figure 4.7, I plot the relationship between the proportions of Oii and Oiii peak intensities and the electron concentration. First, I confirmed that the behavior of the proportion of Oiii peak intensity is inconsistent with the behavior of the electron concentration as shown in Figure 4.7. Figure 4.7, however, demonstrates an interesting behavior of Oii peak intensity. The Oii peak intensity is inversely proportional to the electron concentration; it takes the lowest value (1.3 %) for the film annealed for 30 min and the highest value for the film annealed for 60 min.

Finally, I used the XPS technique to validate the above analysis. Though it has been suggested that the behavior of the Oii peak intensity reveals a direct relation between Oii peak intensity and electron concentration, the interpretation of the Oii peak is still controversial as was noted above. All the values of O1s-related spectral intensities before and after Ar etching of the film surface are summarized in Table 4.4, where films A and B are analyzed. It is seen that, for films A and B, the Oii and Oiii peak intensities are reduced after Ar etching. According to John C. C. Fan's article [82], the Oii peak intensity should take a higher value at

Table 4.4. Estimated relative component proportions (h_G values given in eq. (4.2)).

Film category	Gas (Depo-Anneal)	Oi	Oii	Oiii	Zn2p
A (before etching)	Ar - N_2	15.47 %	1.62 %	3.69 %	79.21 %
A (after etching)	Ar - N_2	15.60 %	0.99 %	2.51 %	80.60 %
B (before etching)	Ar - O_2	15.46 %	2.09 %	4.44 %	78.01 %
B (after etching)	Ar - O_2	16.89 %	1.35 %	1.86 %	79.89 %

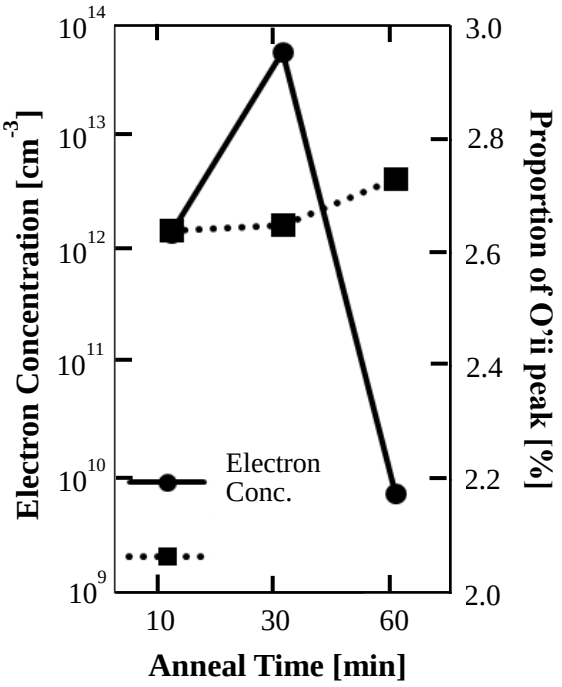

Figure 4.6. Relationship between the O'ii peak height and the electron concentration (film A).

The original O1s spectra are decomposed into two oxygen-related spectral components.

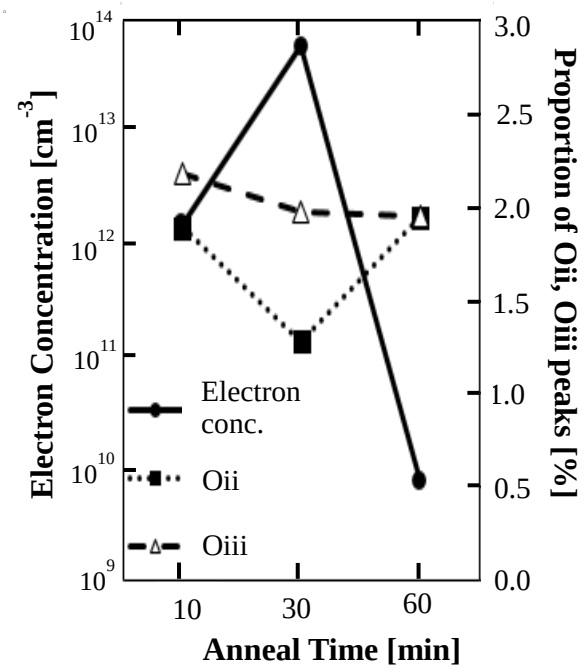

Figure 4.7. Relationship between the Oii peak height or Oiii peak height and the electron concentration (film A).

The original O1s spectra are decomposed into three oxygen-related spectral components.

the surface than in the film body because moisture in the atmosphere can easily diffuse into the film body. In addition, we must address the undesirable effect of carbon-related contamination of the surface of the film prior to annealing. Therefore, I discard the XPS spectra data taken from the surface. In the present experimental results, I consider that the Oii peak extracted from the original spectral profile of the O1s signal is associated with the O^{2-}anions in the ZnO region matrix, and is inversely proportional to electron concentration. It has been discovered that, after Ar etching of the film surface, film B annealed under oxygen gas has much higher Oii peak intensity than film A annealed under nitrogen gas. It is suggested that, in the ZnO matrix region, the film annealed under oxygen gas has much higher oxygen ion concentration than that annealed under nitrogen gas. Due to the excess oxygen ions in the ZnO matrix region, therefore, the oxygen vacancy concentration, which will contribute to the electron generation characteristic of the ZnO film, decreases because the excess oxygen ions, coming from the outside atmosphere, diffuse more deeply into the film and they occupy oxygen vacancy sites.

4.3.5 Examination of the roles of ambient oxygen atoms during deposition

In order to examine the influence of the oxygen ambient in the deposition and anneal processes on the physical property of ZnO films, I used an oxygen isotope (O^{18}) as the ambient gas in the deposition process. I analyzed the depth profiles of oxygen atoms (O^{16} and O^{18}) in the films deposited under the argon/oxygen (O^{18}) mixture gas by the SIMS technique and the bonding states by the XPS technique. The XPS data of various films are shown in Table 4.5. Details of this XPS analysis are given in a later part of this section. The purpose of this experiment is to elucidate the dominant mechanism triggering the different lateral resistance values of ZnO films annealed under nitrogen ambient from those of the ZnO film annealed under oxygen (O^{16}) ambient.

The depth profiles of O^{16}, O^{18}, Zn, Si, and C given by the SIMS analysis are shown in Figure 4.8; Figure 4.8(a) shows the corresponding depth profiles of the as-deposited ZnO film, Figure 4.8(b) those of the ZnO film annealed under nitrogen ambient, and Figure 4.8(c) those of the ZnO film annealed under oxygen (O^{16}) ambient. In Figure 4.8(a), the concentration of O^{18} atoms is similar to that of O^{16} atoms, which reveals that significant amounts of O^{18} atoms were captured by the ZnO film in the deposition process. In Figure 4.8(b)

Table 4.5. Estimated relative component proportions of ZnO films deposited in the Ar/O^{18} mixture ambient (h_G values given in eq. (4.1)). Top surfaces of all samples were etched by Ar^+ beam before the XPS analysis.

Film category	Gas (Depo-Anneal)	Oi	Oii	Oiii	Zn2p
A	Ar - N_2	15.60 %	0.99 %	2.51 %	80.90 %
C	Ar/O_2 - N_2	15.42 %	1.10 %	2.29 %	81.19 %
B	Ar - O_2	16.89%	1.35 %	1.86 %	79.89 %
D	Ar/O_2 - O_2	15.26 %	1.22 %	2.19 %	81.33 %

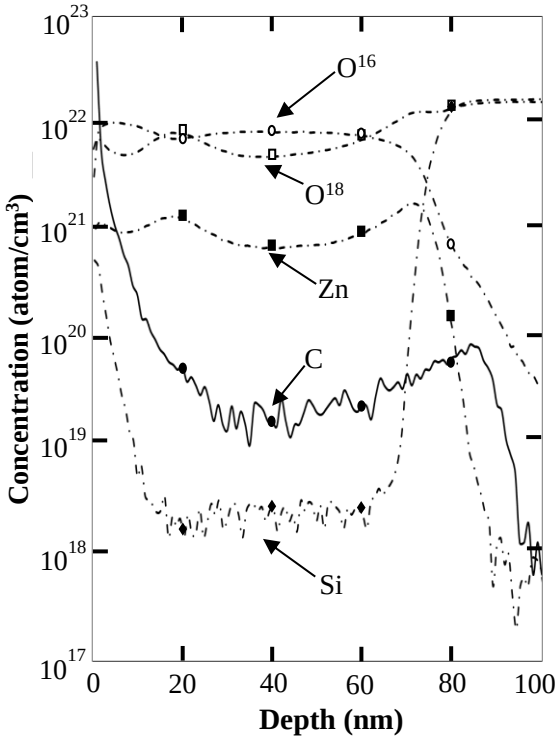
Concentration (atom/cm3)
Depth (nm)
O16
O18
Zn
C
Si

(a)

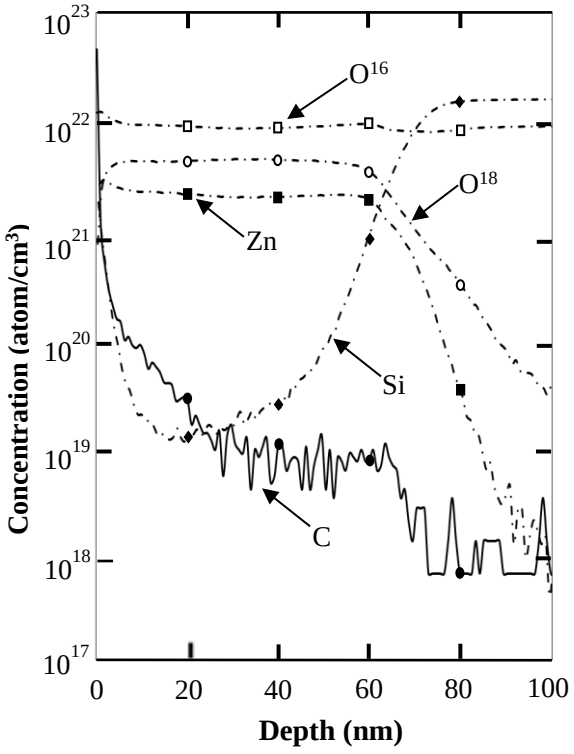
Concentration (atom/cm3)
Depth (nm)
O16
O18
Zn
Si
C

(b)

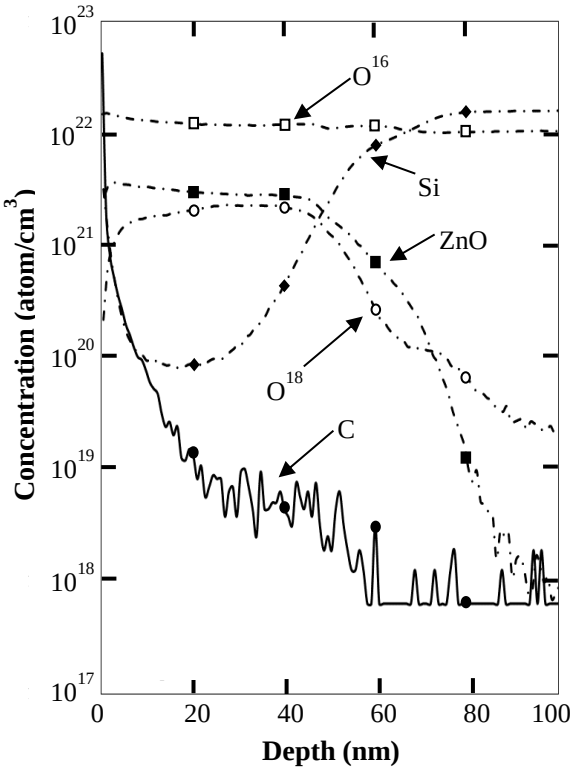

(c)

Fig. 4.8. Depth profiles of atoms (O^{16}, O^{18}, Si, ZnO, and C) in the ZnO films. (a) as-deposited ZnO film, (b) ZnO film annealed in the nitrogen ambient, (c) ZnO film annealed in the oxygen (O^{16}) ambient.

and 4.8(c), it is seen that carbon contamination of the surface is remarkable after the annealing process, so the XPS analysis reliable and useful for discussing the chemical bindings. I also found that the concentration of Si atoms is significantly high for the ZnO film in Figure 4.8(c). It is anticipated that redox of the SiO_2 film has taken place. The influence of SiO_2 film redox must be carefully considered because SiO_2 molecules may be created in the ZnO film.

Figures 4.9 to 4.11 compare the depth profiles of O^{16} and O^{18} atoms for three conditions; Figure 4.9 shows that of the as-deposited ZnO film, Figure 4.10 that of the film annealed under nitrogen ambient, and Figure 4.11 that of the film annealed under oxygen (O^{16}) ambient. After the annealing process under nitrogen ambient, the concentration of O^{18} is slightly decreased, while the concentration of O^{16} is roughly the same as that in Figure 4.9. After the annealing process under oxygen ambient (O^{16}), however, the concentration of O^{18} is significantly decreased and the concentration of O^{16} is increased. It is suggested that the annealing under oxygen ambient (O^{16}) increases the oxygen concentration (O^{16}) of ZnO films, resulting in the decrease in the oxygen vacancy, which is consistent with the measured results for electrical characteristics shown in Figure 4.1 and 4.2. The behavior of O^{18} concentration reveals that the annealing process promotes the out-diffusion of oxygen atoms; O^{18} atoms have the same chemical property as O^{16} atoms [86]. For the annealing process under nitrogen ambient, the out-diffusion of oxygen atoms (O^{18}) should induce the generation of oxygen vacancies. On the other hand, for the annealing process under oxygen ambient, the out-diffusion of oxygen atoms (O^{18}) should be compensated by the diffusion of oxygen molecules (O^{16}) into the ZnO film; the result being a decrease in oxygen vacancies.

The above understanding is consistent with our XPS data summarized in Table 4.5. It is suggested that the films annealed under nitrogen gas have lower Oii peak proportion than those annealed under oxygen gas. The films deposited under Ar/O_2 ambient have higher Oii peak proportion than those deposited under Ar ambient, which suggests that the films deposited under Ar/O_2 ambient have lower oxygen vacancy concentration than those deposited under Ar ambient. This is consistent with our previous discussion that oxygen molecules are captured by the films during deposition if the ambient gas contains oxygen.

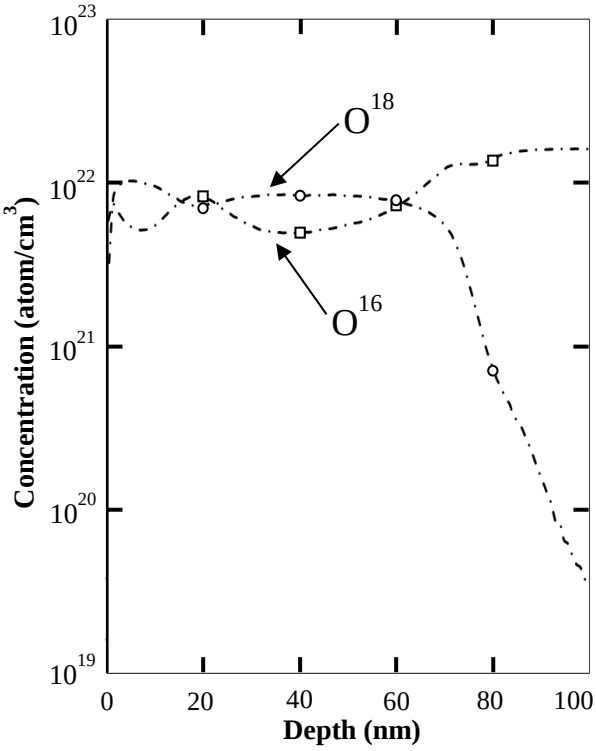

Figure 4.9. Depth profiles of atoms (O^{16} and O^{18}) in the as-deposited ZnO film.

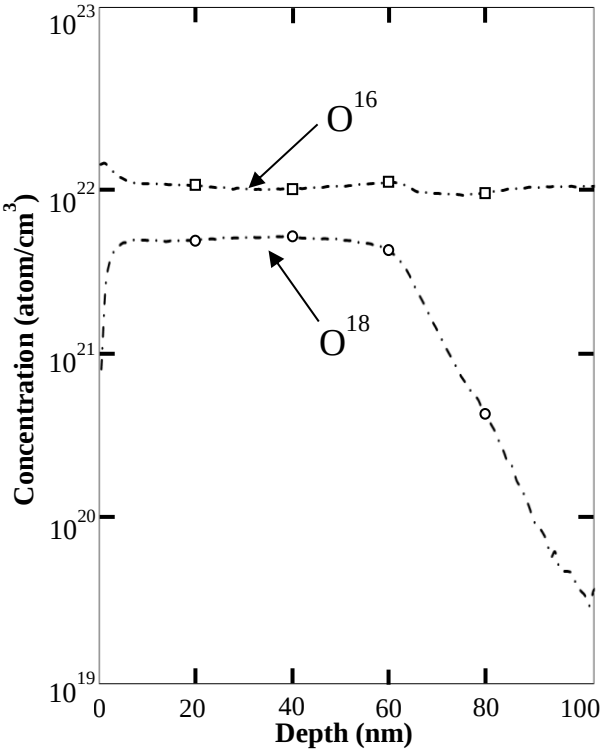

Figure 4.10. Depth profiles of atoms (O^{16} and O^{18}) in the ZnO film annealed in the nitrogen ambient.

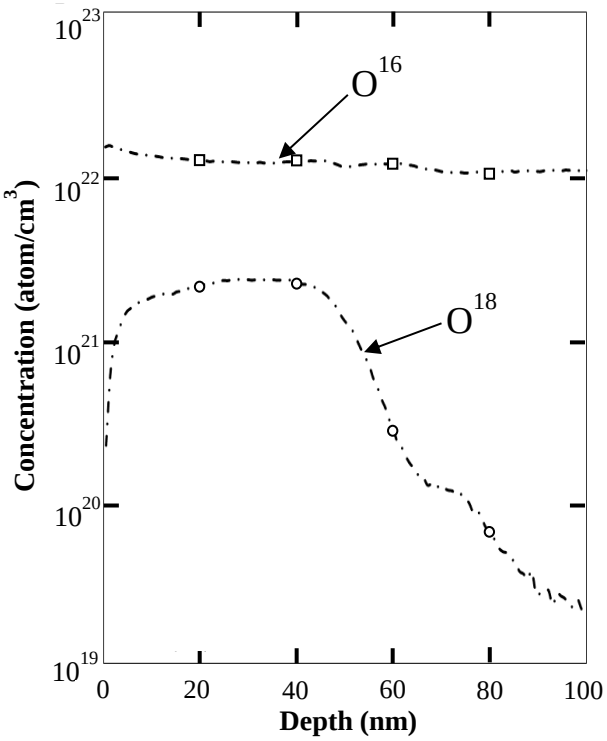

Figure 4.11. Depth profiles of atoms (O^{16} and O^{18}) in the ZnO film annealed in the oxygen (O^{16}) ambient.

Chapter. 5 The Stability of ZnO in Low Humidity

In Chapter 4, I have discussed physical properties of the ZnO and AZO films deposited by using the spin-coated method and possible mechanisms supporting the electrical transport property of the ZnO films deposited by using RF sputtering method. But, in some cases, the environment influences chemical property of ZnO films and changes the electrical property remarkably. For example, the degradation of conductivity of AZO thin film has been reported in a certain ambient, such as, in a high partial oxygen pressure ambient, and in a high humidity ambient. So, in this Chapter, I will discuss the change of electrical property of ZnO films annealed in different atmosphere without the humidity effect as the time goes on.

5.1 Experiment

In this experiment, I used the RF sputtering method which was discussed in Chapter 4.2 in comparison to the spin-coating method; the ZnO films deposited by using RF sputtering method have a more uniform surface and the electrical property is excellent. ZnO films were deposited on P-type silicon substrates with a top SiO_2 film. Before sputtering process, the substrates were cleaned by hydrogen peroxide and concentrated sulfuric acid in three minutes. The deposition pressure was controlled below $4x10^{-3}$ Pa. The RF power density was 1.99 W/cm^2. The distance between the substrate and the ZnO target was 50 mm. The atmosphere of deposition was Ar gas. The as-deposited ZnO films were annealed under nitrogen or oxygen atmosphere for 60 minutes at 700℃, respectively. Then, the humidity stability of the annealed ZnO thin films were tested under a humid ambient. The humidity stability tests were performed in a chamber with the condition of 10 ± 5% humidity at room temperature. In this humidity condition, the effect of humidity can be ignored. The humidity's variation diagram is shown in Fig. 5.1.

I analyzed the surface roughness of ZnO by using AFM (atomic-force microscopy), the in-depth profiles of the normalized atomic ratio values of the ZnO films by using RBS (Rutherford back scattering) technique, surface chemistry of ZnO films by using XPS (X-ray photoelectron spectroscopy), and conductance by using

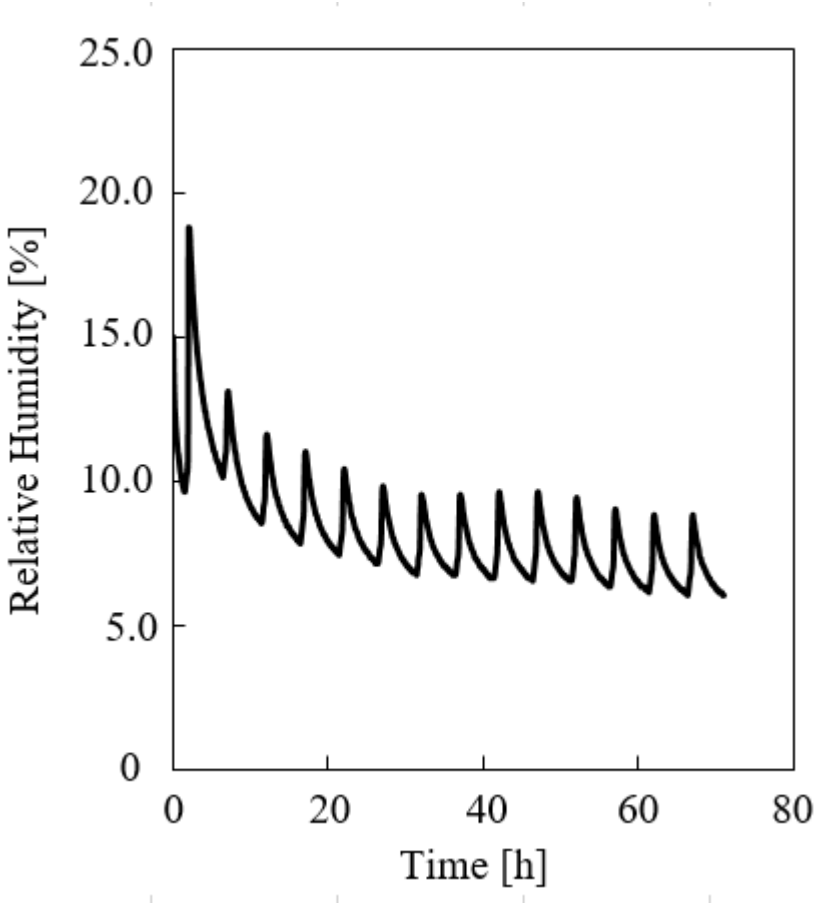

Figure 5.1. The humidity's variation in room temperature.

current-voltage characteristics.

5.2 Result and Discussion

5.2.1 Current - Voltage Characteristics

I measured the d. c. current of nitrogen- or oxygen-annealed ZnO films that was exposed for 23 days in a camber under low humidity environment. Time evolutions of d. c. current valued of ZnO films are shown in Fig. 5.2(a) for the nitrogen-annealed film and Fig. 5.2(b) for the oxygen-annealed film, respectively, where “0 day” means “just after fabrication”. In Fig. 5.2, it is found that the d. c. current of nitrogen-annealed ZnO films shows an ohmic behavior from 0 V to 5 V, on the other hand, the d. c. current of oxygen-annealed ZnO films shows an ohmic behavior from 0 V to 2 V, but being saturation over 2 V regardless of the time exposed under low humidity environment. It seems that the humidity doesn’t influence the electrical transport property of ZnO films. To see clearly about the d. c. current variation of ZnO films, we built a diagram of the conductance at 0.5 V with the time exposure. They are shown in Fig. 5.3. It is found that the conductance of nitrogen-annealed or oxygen-annealed ZnO films is almost stable for 23 days. It seems that the electrical property of ZnO films has not been changed.

5.2.2 AFM Measurement

The surface roughness of oxygen-annealed ZnO films in “0 day” and in “8 day” is shown in Fig. 5.4 (a) and 5.4 (b), respectively. The specific value is shown in Table 5.1. Ra means arithmetic average of absolute values from the center to the edge of the film, Rq means root mean squared value from the center to the edge of the film, and Rmax means a vertical distance from the top to the valley of the film. It is found in Fig. 5.4 that the grain size of the ZnO films for “0day” and “8day” is ranging from 30 nm to 70 nm. It is no definite difference between those films. As, in Table 5.1, values of Ra and Rq in ZnO film for “8day” are larger than those of “0day”, it is inferred that the number of projections of ZnO film surface for “8day” is lower than that for “0day”.

5.2.3 RBS and XPS measurement

The atomic ratios of oxygen-annealed ZnO films exposed for “0day” and “8day” are summarized in Table 5.2, where the atomic ration was evaluated by RBS technique. Since the difference between the two conditions is less than 1% and the accidental error of RBS is approximately 1%, I can’t make a conclusion that the oxygen atomic proportion of ZnO film exposed for “0day” is lower than that for “8day”.

In order to work out this problem, I used the XPS technique to find the atomic proportion of ZnO films. Since the films are readily contaminated by moisture and other chemicals “present in the atmosphere prior to the annealing” during the annealing, I applied the Ar etching technique to remove the film surfaces. The atomic proportion of ZnO films exposed for 0day or for 8day is shown in Table 5.3, where the data was calculated by XPS analysis. It seems that the atomic proportion of ZnO films exposed for 0day is the same as that for 8day.

5.3 Short Summary

In this Chapter, I evaluated the time evolution of electrical property of ZnO films exposed in a low humidity condition for a long time. Although original electrical properties of nitrogen-annealed and oxygen-annealed ZnO films are different, they were basically stable against the air exposure in a low humidity for 23 days. I also analyzed the surface roughness of ZnO films by using AFM (atomic-force microscopy), the in-depth profiles of the normalized atomic ratio values of the ZnO films by using RBS (Rutherford back scattering) technique, and surface chemistry of ZnO films by using XPS (X-ray photoelectron spectroscopy). It was shown that chemical bonding states and atomic ratio of ZnO films were hardly influenced by the air exposure.

Table 5.1. The surface roughness of ZnO films annealed under oxygen atmosphere preserved in 0day or 8day.

Sample	Ra(nm)	Rq(nm)	Rmax(nm)
0day	1.84	2.29	18.6
8day	2.19	2.76	23.2

Table 5.2. The atomic ratios of ZnO films annealed under oxygen atmosphere and preserved in 0day or 8day by RBS technique.

Sample	O/Zn	Ar/Zn
0day	1.02	0.005
8day	0.95	0.005

Table 5.3. The atomic ratios of ZnO films annealed under oxygen atmosphere and preserved in 0day or 8day by XPS technique.

Sample	O (%)	Zn (%)
0day	46.5	53.5
8day	46.4	53.6

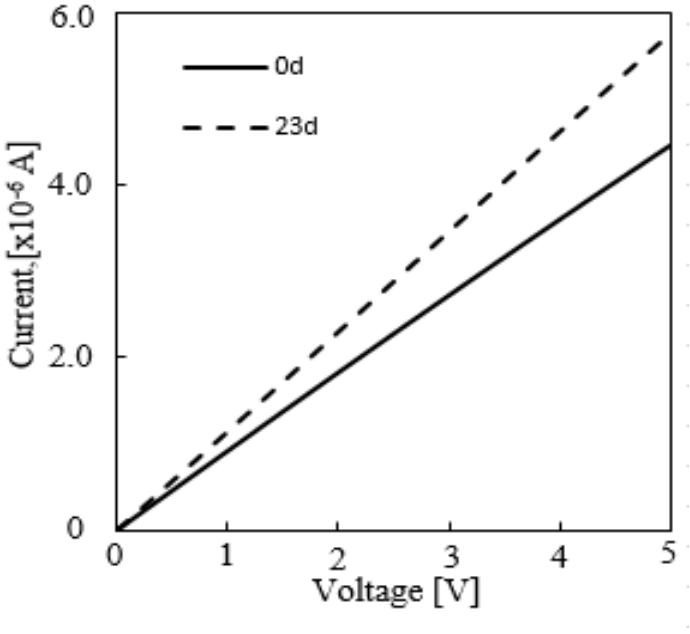

(a) Nitrogen-annealed sample

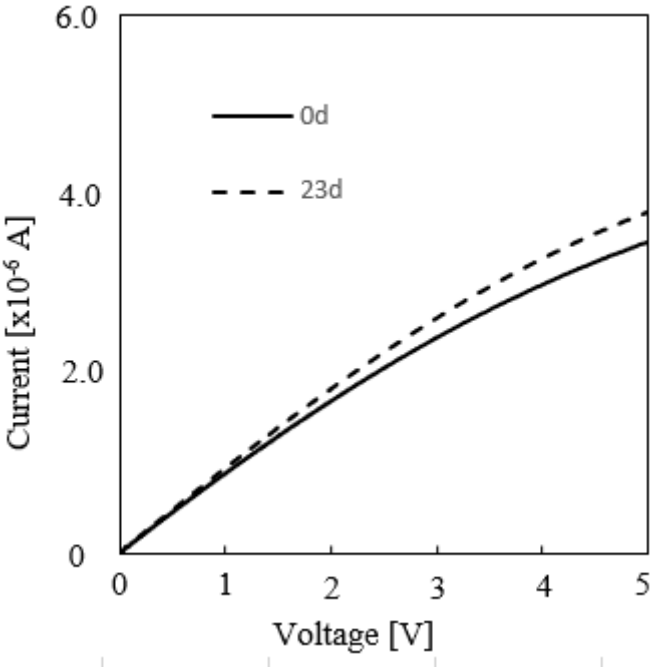

(b) Oxygen-annealed sample

Figure 5.2. Current-Voltage characteristics of ZnO films preserved in 0day and 23day. (a) Annealed under nitrogen atmosphere, (b) Annealed under oxygen atmosphere.

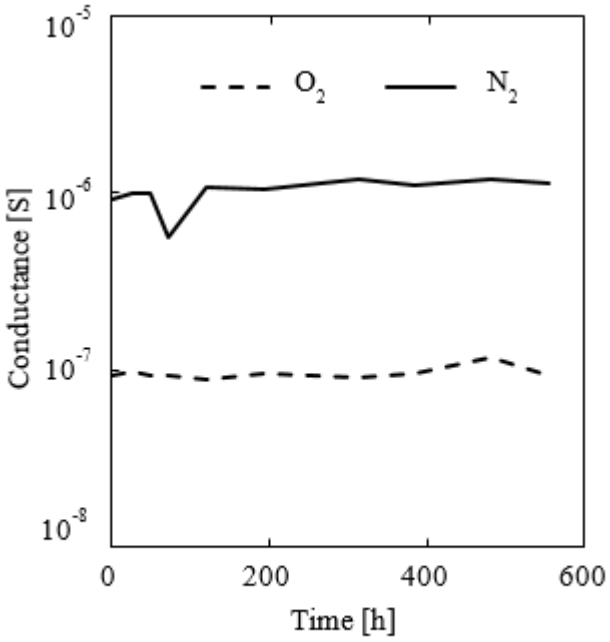

Figure 5.3. The conductance of ZnO annealed under nitrogen or oxygen atmosphere with increasing reserved time in 0.5V.

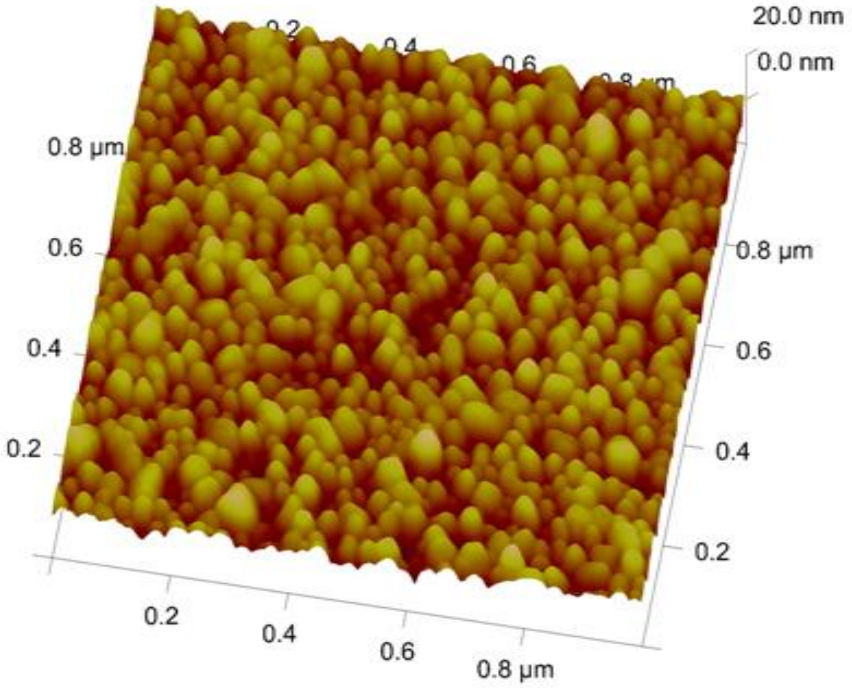

(a) 0day

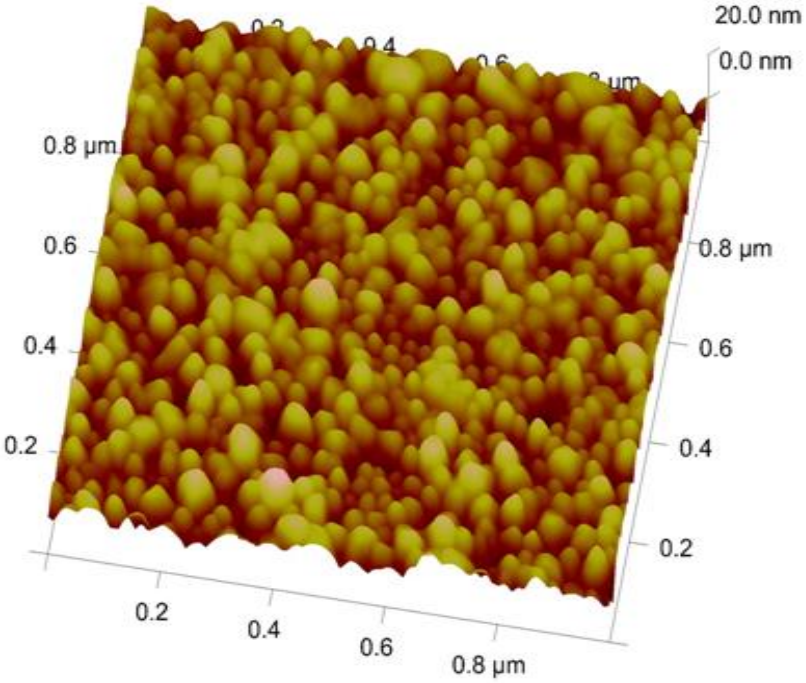

(b) 8day

Figure 5.4. The surface roughness of ZnO films annealed under oxygen.
(a) Preserved in 0day, (b) Preserved in 8day

CHAPTER 6. Conclusion

Currently, indium tin oxide (ITO) thin film is often used as a transparent conductive film in thin film solar cells, flat panel displays, touch-panels and so on. However, indium (In), the raw material of ITO film is a rare metal and toxic, therefore people show great concern about its extensive use. In this context, from an environmental point of view, people pay more and more attention to indium-free material. ZnO thin film is a cheap material and abundant in resources. It is non-toxic and environmentally-friendly. According to theoretical analysis, its resistivity can be expected to reach a value comparable to that of ITO, thus it is considered the most promising alternative material.

In order to improve the electrical properties of ZnO thin film and increase its reproducibility, I discussed the basic physical properties of ZnO film in this dissertation:

[1] Research on the physical properties of ZnO film and aluminum-doped ZnO thin film deposited by using Spin-coating method

In this study, ZnO and Al-doped ZnO (AZO) films were deposited on quartz substrates using spin-coating method. The structural, electrical and optical properties of AZO thin films were investigated. The ZnO and AZO thin films had a hexagonal wurtzite structure and the orientation of the sample was along the c-axis, regardless of annealing temperature. The normalized optical transmittance of ZnO and AZO films decreased with increasing annealing temperature from 400 ℃ to 700 ℃. Since the resistivity of the ZnO films which were deposited by using spin-coating method, it can't be applied to Transparent Conductive Oxide. The resistivity of AZO films decreased with increasing annealing temperature from 400°C to 500°C, but increased with increasing annealing temperature from 500°C to 700°C. These results indicate that increasing the grain size of AZO films will decrease grain boundary scattering so that the resistivity decreases with increasing annealing temperature from 400°C to 500°C. And the lowest resistivity (1.01Ωcm) was obtained at annealing temperature of 500°C in oxygen ambient.

[2] Research on the conductive mechanism of undoped ZnO thin film deposited by using RF sputtering method

Theoretical analysis (first-principles calculation) may not reproduce the physical properties of ZnO, so this research mainly explores into physics in property context in terms of experiment, and makes evaluation on film properties. Undoped ZnO films were deposited on the SiO_2 film of monocrystalline Si substrates by RF sputtering with different deposition conditions and annealing conditions. In this study, we evaluated lateral resistance of the films, crystallinity, chemical bonding states, and chemical stoichiometry in order to elucidate the electron generation mechanism of undoped ZnO films. We found that the films annealed under nitrogen ambient have much lower resistance than those annealed under oxygen ambient. In addition, we proposed that the O1s spectra of ZnO films should be decomposed to three oxygen-related spectral components and that the Oii peak (one of the Gaussian-fitted components extracted from the original O1s spectra) is associated with the O^{2-} anions in the ZnO matrix region because its peak height is inversely proportional to electron concentration. Hence, we think that the Oii peak intensity reflects the amount of oxygen vacancies in the undoped ZnO films. The behavior of depth profiles of oxygen isotope (O^{18}) clearly revealed that the annealing process in the nitrogen ambient promotes the generation of oxygen vacancies, while annealing under oxygen ambient decreases the level of oxygen vacancies. Therefore, it is considered that the behavior of the Oii spectrum intensity is related to the oxygen vacancy level.

[3] Study on stability of ZnO film in low humidity environment

Mass production and durability problems of ZnO thin film have not yet been solved, so it cannot be put into extensive use. In this experiment, we used the RF sputtering method to produce the ZnO films. We measured the current of ZnO films annealed by nitrogen or oxygen from deposited immediately to 23day in a camber under low humidity environment. It is found that the conductance of ZnO films annealed under either nitrogen atmosphere or oxygen atmosphere, is almost consistent from 0day to 23day.

Compared with AFM diagram, it has no obvious different between 0day and 8day. And in atomic ratios of ZnO films annealed under oxygen atmosphere and preserved in 0day or 8day, there is no obvious different between each other. So it is seemed that the electrical property of ZnO films has not been changed even reserved under low humility condition.

REFERENCES

[1] “Electric Energy: An Introduction”, Mohamed A. El-Sharkawi, (CRC Press, 2012), Chapter 1.

[2] “Solar Energy Perspectives: Executive Summary”, produced by International Energy Agency, 2011, pp. 19-22.

[3] Blander. M, S. Sinha, "Calculations of the Influence of Additives on Coal Combustion Deposits", Argonne National Laboratory, pp. 340-346, 1989.

[4] Q. Zhu, J. Sarkis, “An inter-sectoral comparison of green supply chain management in China: Drivers and practices”, J. Cleaner Production, Volume 14, Issue 5, pp. 472–486, 2006.

[5] “Energy: conversion and utilization”, MA, Krenz, J.H.Allyn and Bacon, (Inc.,Boston, , Jan. 1. 1976), Chapter 3.

[6] “Power System Stability and Control”, P. Kundur, (McGraw-Hill, Inc., 1993), Chapter 7.

[7] “The Great Transition: Shifting from Fossil Fuels to Solar and Wind Energy”, Lester R. Brown, with Janet Larsen, J. Matthew Roney, and Emily E. Adams, (Earth Policy Institute, 2015), Chapter 2.

[8] K. Olie, P. L. Vermeulen and O. Hutezinger, “Chlorodibenzo-p-dioxins and chlorodibenzofurans are trace components of fly ash and flue gas of some municipal incinerators in The Netherlands”, Chemosphere, Volume 6, Issue 8, pp.455-459, 1977.

[9] R. M. Navarro, M. A. Peña and J. L. G. Fierro, “Hydrogen Production Reactions from Carbon Feedstocks: Fossil Fuels and Biomass”, Chemical Reviews, Volume 10, Issue 107, pp. 3952-3991, 2007.

[10] “Greenhouse Effect”, B. Bolin and B. R. Doos, (SciTech Connect, 1989), Chapter 1.

[11] “Last change: nuclear proliferation and arms control”, W. Epstein, (SciTech Connect, 1976), Chapter 1.

[12] H. J. Krappe, J. R. Nix and A. J. Sierk, “Unified nuclear potential for heavy-ion elastic scattering, fusion, fission, and ground-state masses and deformations”, Physical Review C, Volume 20, Issue 3, pp. 992-1013, 1979.

[13] S. Shafiee and E. Topal, “When will fossil fuel reserves be diminished?”, Energy Policy, Volume 37, Issue 1, pp.181-189, 2009.

[14] M. Z. Jacobson and M.A. Delucchi, “Providing all global energy with wind, water, and solar power, Part I: Technologies, energy resources, quantities and areas of infrastructure, and materials”, Energy Policy, Volume 39, Issue 3, pp. 1154-1169, 2011.

[15] A. E. Farrell, R. J. Plevin, B. T. Turner, A. D. Jones, M. O'Hare and D. M. Kammen, “Ethanol Can Contribute to Energy and Environmental Goals”, Science, Volume 311, Issue 5760, pp. 506-508, 2006.

[16] P. McKendry, “Energy production from biomass (part 2): conversion technologies”, Bioresourse Technology, Volume 83, Issue 1, pp. 47-54, 2002.

[17] A. A. Goverdovskii, S. G. Kalyakin and V. I. Rachkov, “The alternative strategies of the development of the nuclear power industry in the 21st century”, Thermal Engineering, Volume 61, Issue 5, pp.319-326, 2014.

[18] “Electric Power Systems”, S.A. Nasar and F.C. Trutt, (CRC Press, 1998), Chapter 1.

[19] S. Mathew, A. Yella and etc., “Dye-sensitized solar cells with 13% efficiency achieved through the molecular engineering of porphyrin sensitizers”, Nature Chemistry, Volume 6, pp. 242-247, 2013.

[20] R. R. King, D. C. Law, K. M. Edmondson, C. M. Fetzer, G. S. Kinsey, H. Yoon, R. A. Sherif and N. H. Karam, "40% efficient metamorphic GaInP/GaInAs/Ge multijunction solar cells", Appl. Phys. Letts, Volume 90, pp. 183516-1-183516-3, 2007.

[21] "Fundamentals of Solar Cells", A.L. Fahrenbruch and R.H. Bube, (Academic Press, 1983), Chapter 12.

[22] S.A. Kalogirou, "Solar thermal collectors and applications", Progess in Energy and Combustion Science, Volume 30, Issue 3, pp. 231-295, 2004.

[23] R.W. MilesK, M. Hynes and I. Forbes, "Photovoltaic solar cells: An overview of state-of-the-art cell development and environmental issues", Progress in Crystal Growth and Characterization of Materials, Volume 51, Issue 1-3, pp. 1-42, 2005.

[24] A. Shah, P. Torres, R. Tscharner, N. Wyrsch and H. Keppner, "Photovoltaic Technology: The Case for Thin-Film Solar Cells", Science, Volume 285, Issue 5428, pp. 692-698, 1999.

[25] R.B. Bergmann, "Crystalline Si thin-film solar cells: a review", Appl. Phys. A, Volume 69, Issue 2, pp. 187-194, 1999.

[26] J. Muller and M. Vanecek, "TCO and light trapping in silicon thin film solar cells", Solar Energy, Volume 77, Issue 6, pp. 917-930, 2004.

[27] S. Gao and Y. Xie, "Preparation of $CuAlO_2$ nanocrystalline transparent thin films with high conductivity", Nanotechnology, Volume 14, Issue 5, pp. 221-225, 2003.

[28] A. Mondal and S.K. Bhar, "Galvanic deposition of hexagonal ZnO thin films on TCO glass substrate", Materials Letters, Volume 60, Issue 13-14, pp. 1748-1752, 2006.

[29] S. Su and G. Fang, "p-type transparent conducting oxides", Applications and Materials science, Volume 203, Issue 8, pp.1891-1890, 2006.

[30] N. Ito and Y. Shigesato, "Electrical and optical properties of amorphous indium zinc oxide films", Thin Solid Films, Volume 496, Issue 1, pp. 99-103, 2006.

[31] S.M. Bergin, Y. Chen, and B.J. Wiley, "The effect of nanowire length and diameter on the properties of transparent, conducting nanowire films", Nanoscale, Volume 4, pp.1996-2004, 2012.

[32] J.G. Lu and S. Fujita, "Carrier concentration dependence of band gap shift in n-type ZnO:Al films", J. Appl. Phys., Volume 101, pp. 083705-1-083705-7, 2007.

[33] T. Minami, "New n-Type Transparent Conducting Oxides", MRS Bulletin, Volume 25, Issue 8, pp.38-44, 2000.

[34] T. Yamada and T. Yamamoto, "Effect of thermal annealing on electrical properties of transparent conductive Ga-doped ZnO films prepared by ion-plating using direct-current arc discharge", Thin solid films, Volume 517, Issue 10, pp. 3134-3137, 2009.

[35] J. Yun and J. Kim, "Double transparent conducting oxide films for photoelectric devices", Materials Letters, Volume 70, pp. 4-6, 2012.

[36] N. Sobana and M. Swaminathan, "Nano-Ag particles doped TiO_2 for efficient photodegradation of Direct azo dyes", Journal of Molecular Catalysis A: Chemical, Volume 258, Issue 1-2, pp.124-132, 2006.

[37] S.A. Studenikin, "Fabrication of green and orange photoluminescent, undoped ZnO films using spray pyrolysis", J. Appl. Phys., Volume 84, pp. 2287-1-2287-8, 1998.

[38] X.W. Sun and H.S. Kwok, “Optical properties of epitaxially grown zinc oxide films on sapphire by pulsed laser deposition”, J. Appl. Phys., Volume 86, P. 408-1-408-4, 1999.

[39] S. Fay, “Low pressure chemical vapour deposition of ZnO layers for thin-film solar cells: temperature-induced morphological changes”, Solar Energy Materials and Solar Cells, Volume 86, Issue 3, pp.385-397, 2005.

[40] M. Ohyama and T. Yoko, “Sol-gel preparation of ZnO films with extremely preferred orientation along (002) plane from zinc acetate solution”, Thin Solid Films, Volume 306, Issue 1, pp.78-85, 1997.

[41] C. Lin and H. Lee, “Properties of nitrogen-implanted p-type ZnO films grown on Si_3N_4/$SiSi_3N_4$/Si by radio-frequency magnetron sputtering”, Appl. Phys. Lett.s, Volume 84, pp. 5040-1-5040-3, 2004.

[42] P. Jiang and M.J. McFarland, “Large-Scale Fabrication of Wafer-Size Colloidal Crystals, Macroporous Polymers and Nanocomposites by Spin-Coating”, J. Am. Chem. Soc, Volume126, Issue 42, pp. 13778-13786, 2004.

[43] D.B. Hall and J.M. Torkelson, “Spin coating of thin and ultrathin polymer films”, Volume 38, Issue 12, pp. 2039-2045, 1998.

[44] N. Sahu and S. Panigrahi, “Fundamental understanding and modeling of spin coating process: A review”, Indian Journal of Physics, Volume 83, Issue 4, pp. 493-502, 2009.

[45] “Sol-Gel Technologies for Glass Producers and Users”, D.P. Birnie, (Springer, 2004), Chapter 2.

[46] J. Zhang and K. Nakamura, “Effect of annealing temperature on properties of spin-coated AZO films”, Materials Research Innovations, Volume 18, Issue S4, pp. 674-676, 2014.

[47] U. Helmersson and J.T. Gudmundsson, “Ionized physical vapor deposition (IPVD): A review of technology and applications”, Thin Solid Films, Volume 513, Issue 1-2, pp. 1-24, 2006.

[48] “Transparent Conductive ZnO Oxide”, R. Hull and etc., (Springer, 2008), Chapter 5.

[49] K. Brand, “The reflected beam spR.O Films”, ECS Journal of Solid State Science and Technology, Volume 10, Issue 5, pp. 565-571, 2016.

[51] R. Hong and J. Shao, “Influence of different post-treatments on the structure and optical properties of zinc oxide thin films”, Applied Surface Science, Volume 242, Issue 3-4, pp. 346-352, 2005.

[52] “Physics of Semiconductor Devices”, S.M. Sze, (Wiley Interscience, 2007), Chapter 1.

[53] U. Holzwarth and N. Gibson, “The Scherrer equation versus the 'Debye-Scherrer equation'”, Nature Nanotechnology, Volume 534, Issue 6, pp. 28-34, 2011.

[54] G. Zaccanti and P. Bruscaglioni, “Deviation from the Lambert-Beer Law in the Transmittance of a Light Beam Through Diffusing Media: Experimental Results”, Journal of Modern Optics, Volume 35, Issue 2, pp. 229-242, 1987.

[55] M. Yang and G. Chen, “High-temperature steam reforming of methanol over ZnO–Al_2O_3catalysts”, Applied Catalysis B: Environmental, Volume 101, Issue 3-4, pp.409-416, 2011.

[56] K.E. Lee, M. Wang, E.J. Kim, and S.H. Hahn, “Structural, electrical and optical properties of sol–gel AZO thin films”, Current Applied Physics, Volume 9, pp.683-687, 2009.

[57] J. C. Manifacier; J. Gasiot and J. P. Fillard, “A simple method for the determination of the optical constants n, k and the thickness of a weakly absorbing thin film”, Journal of Physics E: Scientific Instruments, Volume 9, pp.1002-1004, 1976.

[58] E. Burstein, “Anomalous Optical Absorption Limit in InSb”, Physics Review, Volume 93, Issue 3, pp. 632-633, 1954.

[59] Z. L. Pei, C. Sun, M. H. Tan, J. Q. Xiao, D. H. Guan, R. F. Huang, and L. S. Wen, “Optical and electrical properties of direct-current magnetron sputtered ZnO: Al films”, J. Appl. Phys., Volume 90, pp.3421-1-3421-5, 2001.

[60] A. Janotti and C. G. Van de Walle, “Oxygen vacancies in ZnO”, Appl. Phys. Lett., Volume 87, pp.122102-1-122102-3, 2005.

[61] H. S. Kang, J. S. Kang, J. W. Kim and S. Y. Lee, “Annealing effect on the property of ultraviolet and green emissions of ZnO thin films”, J. Appl. Phys., Volume 95, pp. 1246-1-1246-5, 2004.

[62] C. H. Park, S. B. Zhang, and Su-Huai Wei, “Origin of *p*-type doping difficulty in ZnO:The impurity perspective”, Phys. Rev. B, Volume 66, pp. 073202-1-073202-3, 2002.

[63] K. Vanheusden, C. H. Seager, W. L. Warren, D. R. Tallant, and J. A. Voigt, “Correlation between photoluminescence and oxygen vacancies in ZnO phosphors”, Appl. Phys. Lett., Volume 68, pp. 403-1-403-3 , 1996.

[64] C. G. Van der Walle, “Hydrogen as a Cause of Doping in Zinc Oxide”, Phy. Rev. Lett., Volume 85, pp.1012-1015, 2000.

[65] N. Ohashi, T. Ishigaki, N. Okada, T. Sekiguchi, I. Sakaguchi and H. Haneda, “Effect of hydrogen doping on ultraviolet emission spectra of various types of ZnO”, Appl. Phys. Lett., Volume 80, pp. 2869-1-2869-3, 2002.

[66] F. A. Selim, M. H. Weber, D. Solodovnikov, and K. G. Lynn, “Nature of Native Defects in ZnO”, Phys. Rev. Lett., Volume 99, pp.085502-1-085502-4, 2007.

[67] J. Cui, “Zinc oxide nanowires”, Material Characterization, Volume 64, pp.43-52, 2012.

[68] Y. Du and F. Zeng, “Annealing effects on the cathodoluminescence properties of individual ZnO nanowire”, Materials Lett., Volume 65, Issue 14, pp.2238-2240, 2011.

[69] J. Fang, Y. Hao, C. Munuera, M. Garcia-Hernandez, F. Guoell, E. M. J. Johansson, G. Boschloo, A. Hagfeldt, and A. Cabot, “Influence of the Annealing Atmosphere on the Performance of ZnO Nanowire Dye-Sensitized Solar Cells”, J. Phys. Chem., Volume 117, Issue 32, pp.16349-16356, 2013.

[70] “Polycrystalline silicon for integrated circuit applications”, T. Kamins, (Norwell, MA: Kluwer Academic Pub., 1988), pp.178.

[71] J. M. Bian, X. M. Li, X. D. Gao , W. D. Yu and L. D. Chen, “Deposition and electrical properties of N–In codoped p-type ZnO films by ultrasonic spray pyrolysis”, Appl. Phys. Lett., Volume 84, pp.541-1-541-3, 2004.

[72] M. Chen, X. Wang, Y. H. Yu, Z. L. Pei, X. D. Bai, C. Sun, R. F. Huang, and L. S. Wen, “X-ray photoelectron spectroscopy and auger electron spectroscopy studies of Al-doped ZnO films”, Appl. Surf. Sci., Volume 158, Issue 1-2, pp.134-140, 2000.

[73] L. W. Yang, X. L. Wu, G. S. Huang, T. Qiu and Y. M. Yang, “In situ synthesis of Mn-doped ZnO multileg nanostructures and Mn-related Raman vibration “, J. Appl. Phys., Volume 97, pp.014308-1-014308-4, 2005.

[74] M. N. Islam, T. B. Ghosh, K. L. Chopra, and H. N. Acharya, “XPS and X-ray diffraction studies of aluminum-doped zinc oxide transparent conducting films”, Thin Solid Films, Volume 280, Issue 1-2, pp.20-25, 1996.

[75] Y. Choi, G. H. Kim, W. H. Jeong, J. H. Bae, H. J. Kim, J. Hong, and J. W. Yu, "Carrier-suppressing effect of scandium in InZnO systems for solution-processed thin film transistors", Appl. Phys. Lett., Volume 97, pp.162102-1-162102-3, 2010.

[76] J. H. Kang, E. N. Cho, C. E. Kim, M. Lee, S. J. Lee, J. Myoung, and I. Yun, "Mobility enhancement in amorphous InGaZnO thin-film transistors by Ar plasma treatment", Appl. Phys. Lett., Volume 102, pp.222103-1-222103-3, 2013.

[77] M. Chen, Z.L. Pei, C. Sun, L.S. Wen, X. Wang, "Surface characterization of transparent conductive oxide Al-doped ZnO films", J. Cryst. Growth, Volume 220, Issue 3, pp.254-262, 2000.

[78] K. A. Bogle, M. N. Bachhav, M. S. Deo, N. Valanoor, and S. B. Ogale, "Enhanced nonvolatile resistive switching in dilutely cobalt doped TiO_2", Appl. Phys. Lett., Volume 95, pp.203502-1-203502-3, 2009.

[79] W. J. Ma, S. P. Lin, J. M. Luo, X. Y. Zhang, Y. Wang, Z. X. Li, B. Wang, and Y. Zheng, "Highly uniform bipolar resistive switching characteristics in $TiO_2/BaTiO_3/TiO_2$ multilayer", Appl. Phys. Lett., Volume 103, pp.262903-1-262903-5, 2013.

[80] G. Gaggiotti, A. Galdikas, S. Kaciulis, G. Mattogno, and A. Setkus, "Surface chemistry of tin oxide based gas sensors", J. Appl. Phys., Volume 76, pp.4467-1-4467-5, 1994.

[81] A. Aronniemi, J. Sainio, and J. Lahtinen, "XPS study on the correlation between chemical state and oxygen-sensing properties of an iron oxide thin film", Appl. Surf. Sci., Volume 253, Issue 24, pp.9476-9482, 2007.

[82] J. C. C. Fan and J. B. Goodenough, "X‐ray photoemission spectroscopy studies of Sn‐doped indium oxide films", J. Appl. Phys., Volume 48, pp.3524-1-3524-7, 1977.

[83] X. Q. Wei, B. Y. Man, M. Liu, C. S. Xue, H. Z. Zhuang, and C. Yang, "Blue luminescent centers and microstructural evaluation by XPS and Raman in ZnO thin films annealed in vacuum, N2 and O2", Physica B, Volume 388, Issue 1-2, pp.145-152, 2007.

[84] Y. F. Lu, H. Q. Ni, Z. H. Mai and Z. M. Ren, "The effects of thermal annealing on ZnO thin films grown by pulsed laser deposition", J. Appl. Phys., Volume 88, pp.498-1-498-5, 2000.

[85] X. L. Wu, G. G. Siu, C. L. Fu and H. C. Ong, "Photoluminescence and cathodoluminescence studies of stoichiometric and oxygendeficient ZnO films", Appl. Phys. Lett., Volume 78, pp.2285-1-2285-3, 2001.

[86] "Introductory chemistry", D. D. Ebbing, (Boston: Houghton Mifflin, 1995), Chapter 3.

Acknowledgements

I would like to express my sincere thanks to Prof. Yasuhisa Omura (Dept. Electric, Electronics, and Information Eng., Kansai University), Prof. Tadashi Sakitoh (Dept. Physics and Applied Physics, Kansai University), and Prof. Yoshiro Tjitsu (Dept. Electric, Electron. And Information Eng., Kansai University) for their successive instruction and guidance throughout the study. In addition, I also express my thanks to Mr. Naoto Takahashi for his technical assistance on electrical measurements and optical measurements.

Finally, I am indebted to my parents and my wife for their continuous support and encouragement.